# Single-cell RNA profiling of *Plasmodium vivax* liver stages reveals parasite- and host-specific transcriptomic signatures and drug targets

Anthony A Ruberto [a], Steven P Maher [a], Amélie Vantaux [b], Chester J Joyner [a,c], Caitlin Bourke [d], Balu Balan [d,e] , Aaron Jex [d,e], Ivo Mueller [d] , Benoit Witkowski [b], Dennis E Kyle [a]

[a] Center for Tropical and Emerging Global Diseases, University of Georgia, Athens, GA, United States

[b] Malaria Molecular Epidemiology Unit, Institut Pasteur du Cambodge, Phnom Penh, Cambodia

[c] Department of Infectious Diseases, College of Veterinary Medicine, University of Georgia, Athens, GA, USA

[d] Population Health & Immunity Division, Walter and Eliza Hall Health Institute, Parkville, Victoria, Australia

[e] Faculty of Veterinary and Agricultural Sciences, University of Melbourne, Parkville, Victoria, Australia

Running Head: Single-cell RNA profiling of *P. vivax* liver stages

Address correspondence to dennis.kyle@uga.edu

## ABSTRACT

The resilience of *Plasmodium vivax*, the most widely distributed malaria-causing parasite in humans worldwide, is attributed to its ability to produce dormant liver forms known as hypnozoites, which can activate weeks, months, or even years after an initial mosquito bite. The factors underlying hypnozoite formation and activation are poorly understood, as is the parasite's influence on the host hepatocyte. Here, we shed light on transcriptome-wide signatures of both the parasite and the infected host cell by sequencing over 1,000 *P. vivax* liver forms at single-cell resolution. We distinguish between replicating schizonts and hypnozoites at the transcriptional level, identifying key differences in transcripts encoding for RNA-binding proteins associated with cell fate. In infected hepatocytes, we show that genes associated with energy metabolism and antioxidant stress response were upregulated, and those involved in the host immune response downregulated, suggesting both schizonts and hypnozoites alter the host intracellular environment. The transcriptional markers in schizonts, hypnozoites, and infected hepatocytes revealed here pinpoint potential factors underlying dormancy and can inform drug targets against *P. vivax* liver-stage infection.

## IMPORTANCE

In humans, malaria-causing *Plasmodium* parasites invade and replicate in the liver before mounting an infection in the blood. A few *Plasmodium* species, including *P. vivax*, can cause relapsing infections due to forms that persist in the liver known as hypnozoites. While interventions targeting the hypnozoite can prevent clinical malaria, little is known about their biology at the molecular level. Transcriptome-wide assessment of individual hypnozoites has not been accessible due to the technical challenges associated with liver stage infections. To overcome technical limitations, we performed single-cell transcriptional profiling of liver stages generated using an *in vitro* infection platform. In elucidating the transcriptional signatures of *P. vivax* liver forms, as well as hepatocytes in response to infection, our data provide new insights into these host-parasite interactions. An improved understanding of these interactions will allow for novel drug or vaccine interventions targeting either parasite- or hepatocyte-specific metabolic pathways essential for successful liver stage development and disease progression.

## INTRODUCTION

Malaria is a significant global health burden, with an estimated 421 million cases and 627,000 deaths per year (World Health Organization, 2021). At least five *Plasmodium* species are known to infect humans, with *P. vivax* being responsible for the majority of cases outside Africa (World Health Organization, 2021). All *Plasmodium* parasites that infect humans have an obligatory developmental stage in the liver wherein the parasite undergoes asexual reproduction known as schizogony within a

49 hepatocyte before releasing thousands of merozoites into the blood. In *P. vivax*, a proportion of parasites
50 known as hypnozoites forgo immediate division in hepatocytes, and persist in the liver for weeks,
51 months, or years before activating to initiate schizogony resulting in a relapse blood infection (Adams
52 and Mueller, 2017; Krotoski et al., 1982). Hypnozoites are thought to cause up to 90% of cases in certain
53 geographical regions (Adekunle et al., 2015; Commons et al., 2020; Robinson et al., 2015), and
54 mathematical models predict that eliminating *P. vivax* malaria will be difficult without interventions that
55 target hypnozoite reservoirs (White et al., 2018).

56 The factors influencing the biogenesis, persistence, and activation of hypnozoites are poorly
57 understood. Studies have found that hypnozoites in temperate regions have long latencies and that
58 tropical ones have short latencies, suggesting a correlation between geographical region and relapse
59 patterns ((Battle et al., 2014; Huldén et al., 2008; Krotoski et al., 1986; White, 2011). These findings
60 suggest that the developmental trajectory is genetically encoded, and support the hypothesis that
61 developmental fate is somehow pre-programmed in the sporozoite (Lysenko et al., 1977; Ungureanu et
62 al., 1976); but other contributing factors from the host could play a role in determining whether the
63 sporozoite becomes a schizont or hypnozoite (Schäfer et al., 2021).

64 Our understanding of *P. vivax* liver stage biology at the cellular and molecular level is in its
65 nascency for two overarching reasons. For a long time, protocols to cryopreserve and continuously
66 maintain erythrocytic stage parasites *in vitro* were lacking, which necessitated the collection of
67 gametocyte-infected blood from human volunteers in *P. vivax* malaria-endemic regions to generate the
68 sporozoites required to initiate an infection. New laboratory models have recently been developed which
69 can partially alleviate the need to obtain gametocytes from human infected blood (Mikolajczak et al.,
70 2015; Schäfer et al., 2020). In addition to the sporozoite limitation, upon infecting the liver the high
71 ratio of noninfected versus infected hepatocytes has historically made it difficult to isolate and study
72 these forms in sufficient numbers. Robust *in vitro* pre-erythrocytic platforms capable of long-term
73 culture of sufficient numbers of *P. vivax* liver stages have only recently been developed (Maher et al.,
74 2021; Roth et al., 2018). Much of our knowledge of hypnozoite biology at the molecular level remains
75 limited to studies using *P. cynomolgi*—a parasite capable of causing relapsing infections non-human
76 primates, and for which molecular tools are available (Chua et al., 2019; Cubi et al., 2017; Voorberg-
77 van der Wel et al., 2017, 2020). However, it is unknown whether mechanisms regulating hypnozoite
78 formation and dormancy are consistent across different relapsing malaria parasites.

79 Transcriptome-wide profiling of *P. vivax* liver stages has previously been performed using a
80 bulk RNA sequencing strategy (Gural et al., 2018).While informative, the data only provide insights
81 into average transcript levels derived from either mixed (schizont and hypnozoite) or hypnozoite-only
82 populations, masking any transcriptional variation that might exist between individual parasites. Second,

83 the parasite's potential impact on the hepatocyte is not considered, barring analysis of host-pathogen
84 interactions. Nevertheless, these shortcomings highlight a need to better understand differences between
85 individual parasites, as well as how the parasite alters the hepatocyte. Advancements in these areas could
86 help elucidate parasite- and host- factors important for the parasite's liver stage development.

87 Single-cell RNA-sequencing (scRNA-seq) methods offer new ways of studying cell-to-cell
88 variation (Aldridge and Teichmann, 2020), and have already allowed for novel insights into host-
89 pathogen interactions in various disease contexts (Penaranda and Hung, 2019). In *Plasmodium* spp.,
90 scRNA-seq analyses have so far revealed that individual parasite forms exist on a spectrum
91 of transcriptomic states (Bogale et al., 2021; Howick et al., 2019; Poran et al., 2017; Real et al., 2021;
92 Reid et al., 2018; Ruberto et al., 2021a), and applying them to study the biology of *P. vivax* is a
93 burgeoning area of research (Mancio-Silva et al., 2021; Ruberto et al., 2021b; Sà et al., 2020). Droplet-
94 based techniques, such as 10x Genomics (Zheng et al., 2017), which use microfluidics, allow for the
95 sequencing of tens to hundreds of thousands of cells, increasing the chances of observing rare cell
96 populations (e.g., hepatocytes infected with *P. vivax*). We therefore presumed that applying single-cell
97 sequencing to *P. vivax* liver forms derived using an *in vitro* platform would prove a fruitful avenue of
98 inquiry into the parasite's biology cellular and molecular levels.

99 Using scRNA-seq, we characterize transcriptomic signatures of parasite and host in an *in vitro*
100 *P. vivax* liver stage model. We find differences in gene expression between replicating schizonts and
101 hypnozoites, and reveal variation, previously unobservable by bulk sequencing approaches, between
102 individual hypnozoites. In infected hepatocytes, we find that genes associated with energy metabolism
103 and antioxidant stress response are upregulated, and those involved in the host immune response
104 downregulated. Various host genes associated with these processes are found to be exclusively
105 upregulated during hypnozoite infection. Our study elucidates the transcriptional signatures among
106 infected hepatocytes and presents potential mechanisms *P. vivax* can use to either exploit its host for
107 rapid proliferation or to quietly persist, remaining undetected by the host immune system.

## 108 RESULTS

### 109 Strategy used to study *P. vivax* liver stage biology

110 Primary human hepatocytes were cultured and infected with *P. vivax* sporozoites on a 384-well plate
111 platform (Maher et al., 2021; Roth et al., 2018). **Figure 1A** outlines the workflow for the experiment.
112 Following infection with sporozoites, cultures were assessed at two endpoints: one containing both
113 schizonts and hypnozoites at day 5 post-infection, and the other containing solely hypnozoites at day 9
114 post-infection. Schizonts were eliminated from day 9 post-infection cultures by adding the

115 phosphatidylinositol 4-kinase (PI4K) inhibitor MMV390048 (1 μM) to the culture media on days 5, 6
116 and 7 post-infection (Gural et al., 2018; Paquet et al., 2017). For each collection time point, we
117 simultaneously initiated two sets of hepatocyte cultures: one infected with sporozoites for quantification
118 of immunofluorescent-labeled parasites by high-content imaging (HCI), and one infected with
119 sporozoites for transcriptional profiling using a high-throughput, droplet-based scRNA-seq workflow
120 (Zheng et al., 2017). As controls, a third set of naïve cultures were left uninfected and processed for
121 scRNA-seq alongside cultures at days 5 and day 9 post-infection. At each collection point, a target of
122 approximately 10,000 individual hepatocytes were partitioned into droplets prior to the generation of
123 RNA libraries. Each droplet contained primers with a unique cellular barcode that was ligated to
124 transcripts during the reverse transcription step, allowing for the identification of each transcript's
125 cellular origin post-sequencing. After sequencing the single-cell libraries, we mapped the resulting reads
126 onto the human (Ensembl, v103) and *P. vivax* PVP01 (PlasmoDB, v51) transcriptomes. We combined
127 the transcript information with the cellular barcodes to assess the number of transcripts in each cell, and
128 to determine whether a hepatocyte contained parasite material.

129 As expected, we detected hepatocytes infected with both forms of the parasite at 5 days post-
130 infection, and only hypnozoites at 9 days post-infection following exposure to MMV390048 (**Fig. 1B**
131 **and Fig. S1A**). **Figure 1C** displays the distribution of individual parasite growth areas, number of
132 parasites detected, and parasitemia levels at each endpoint. Across replicates, the parasitemia ranged
133 from 5.50-6.93% at 5 days post-infection and 1.76-2.77% at 9 days post-infection. Together, the high
134 infection rates coupled with the high-throughput capacity of 10x Genomics' single-cell isolation and
135 sequencing workflow allowed for sufficient material to be generated for successful profiling of both
136 parasite and host transcriptomes.

137 ***P. vivax* schizonts and hypnozoites are distinguishable at single-cell resolution**

138 We first analyzed the reads mapping to the *P. vivax* transcriptome to identify schizonts and hypnozoites,
139 as well as to assess the extent to which these forms differed at single-cell resolution. In total, we
140 characterized 1,438 parasite transcriptomes across two independent experimental replicates (**Fig. S1B**).
141 The number of parasite transcriptomes profiled corroborated the parasitemia levels quantified using
142 high-content imaging (**Table S1**). Low dimensional representation of the data revealed two populations
143 of parasites in samples profiled at 5 days post-infection (**Fig. 2A, left panel**). In contrast, and as
144 expected, samples profiled at 9 days post-infection contained one population (**Fig. 2A, right panel**).
145 Given that the population of cells profiled at day 9 post-infection, from which schizonts were chemically
146 removed, overlapped with one of the two cell populations profiled at 5 days post-infection, we deduced
147 that non-overlapping population of cells encoded for schizonts. Consistent with our reasoning, an
148 unsupervised clustering algorithm (Traag et al., 2019) unbiasedly assigned the cells to one of the two

149 clusters (**Fig. 2B and Fig. S1C**). As expected, number of transcripts detected, unique molecular
150 identifier (UMI) counts (a readout for absolute transcript abundances (Kivioja et al., 2011), and the
151 transcript levels of the early liver stage development marker liver stage-specific protein, LISP2
152 (PVP01_0304700) (Gupta et al., 2019), all displayed greater quantities in the schizont cluster (C2)
153 relative to the hypnozoite cluster (C1) (**Fig. 1C**). Together, these findings show that the transcriptomes
154 of *P. vivax* schizonts and hypnozoites can be distinguished using our experimental workflow.

155 **Hypnozoites exhibit distinct transcriptional signatures compared to schizonts**

156 We next performed differential gene expression analysis to identify transcriptome-wide differences
157 distinguishing schizonts and hypnozoites. Using stringent inclusion cutoffs (adjusted p value < 0.01 &
158 absolute (average $\log_2$ fold change [FC]) > 0.5), we found significant differences in ~18% (836/4722)
159 of all transcripts detected (**Fig. S2A; Table S2**). Relative to hypnozoites, we found an increase in the
160 expression levels of 368 genes in schizonts. As expected, we observed a significant increase of LISP2
161 in schizonts (average $\log_2$ FC: 2.32) compared to hypnozoites. Shortly after invading the hepatocyte,
162 non-relapsing *Plasmodium* spp. liver forms undergo immediate replication. Studies in rodent malaria
163 models have shown that these forms are metabolically active and that various genes involved in energy
164 metabolism are upregulated (Caldelari et al., 2019; Tarun et al., 2008; Toro-Moreno et al., 2020).
165 Consistent with previous data, we found an increased transcription associated with glycolysis
166 (PVP01_0816000, PVP01_1229700, PVP01_1244000) and the TCA cycle (PVP01_0106100,
167 PVP01_1332400) in schizonts (**Fig. S2B; Table S2**). More broadly, we found increased transcription
168 of various metabolic processes, as well as motility, DNA-, RNA-, and protein-processing (**Fig. S2C;**
169 **Table S2**). Transcripts encoding for various proteasome subunits displayed greater transcription in
170 schizonts (**Fig. S3A; Table S2**). To further show the importance of this protein complex, we tested a
171 known proteosome inhibitor, Carfilzomib (Kortuem and Stewart, 2013), in our standard 12-day *P. vivax*
172 small molecule screening assay (Maher et al., 2021), and found it effectively killed schizonts ($IC_{50}$
173 288nM) and hypnozoites ($IC_{50}$ 511nM) with some selectivity over host hepatocytes ($IC_{50}$ 3.32 μM)
174 (**Figs. S3B and S3D**).

175 The detection of transcripts associated with energy metabolism in hypnozoites, albeit at a lower
176 level relative to schizonts, suggested that these forms are also metabolically active (**Fig. S2B**). Relative
177 to replicating schizonts, we found an increase in gene expression of 468 transcripts in hypnozoites
178 (**Table S2**). As represented in **Figure 3A**, genes with greater expression in hypnozoites encoded for a
179 diverse set of ontologies—including proteases, membrane proteins, transcription factors, and DNA-
180 /RNA-regulating proteins. Genes encoding for proteases vivapain-1, vivapain-2 (PVP01_1248900,
181 PVP01_0916200), and plasmepsin IV (PVP01_1340900) displayed the greatest differential expression
182 in these forms compared to schizonts (**Figs. 3A and 3B, Table S2**). While limited research has reported

183 the functionality of these gene products in *P. vivax* (Byoung-Kuk et al., 2004), work in other
184 *Plasmodium* spp. has revealed that they localize to the food vacuole and play an important role in
185 hemoglobin catabolism during the blood stages of the parasite's life cycle (Dame et al., 2003; Drew et
186 al., 2008).

187 We also identified genes with greater expression associated with RNA regulatory mechanisms.
188 Notably, we found greater expression of CCR4 (PVP01_1429000), a transcript encoding for a protein
189 shown to have mRNA deadenylase activity and play a role in mRNA turnover (Tucker et al., 2001)
190 (**Table S2**). In *Plasmodium* spp., it has been described as important in regulating the expression of genes
191 associated with invasion and egress in blood stages (Balu et al., 2011). RNA-binding proteins (RBPs)
192 also govern gene expression at the post-transcriptional level by transiently storing transcripts until later
193 processing (Hentze et al., 2018). Pumilio domain (PUF) proteins are a major family of RBPs that
194 regulate cellular fating through translational repression in eukaryotes. We found that the transcript
195 encoding for PUF1 (PVP01_1015200) was detected almost exclusively in hypnozoites (**Figs. 3A and**
196 **3B**; **Table S2**). Furthermore, we found greater expression of 7-Helix-1 protein (PVP01_1008400) (**Figs.**
197 **3A and 3B**; **Table S2**)—a stress granule component that interacts with the RNA-binding protein PUF2
198 and serves to be crucial for protein synthesis in *P. falciparum* (Miao et al., 2010). Numerous studies
199 have shown that *Plasmodium* spp. use various post-transcriptional regulatory mechanisms to coordinate
200 stage transitions and development (Baumgarten et al., 2019; Bunnik et al., 2016; Foth et al., 2011; le
201 Roch et al., 2004; Tarun et al., 2008; Vembar et al., 2016). Our data corroborate these findings and
202 suggest that similar strategies may be used in *P. vivax* to regulate liver stage development. Moreover,
203 these data suggest that RBP-mediated cellular fating and translational repression may be involved in
204 regulating hypnozoite dormancy.

205 Given the potential role in RBP-mediated cellular fating and translational repression governing
206 latency in hypnozoites, we performed further analyses focused on RBP-mediated regulation. To this
207 end, we scanned the *P. vivax* genome searching for genes encoding for cellular fating RBPs based on
208 ortholog groups (OGs) of known human cellular fating RBPs (348 RBPs; 227 OGs), identifying around
209 89 OGs (99 RBPs) in *P. vivax.* We detected 48 genes encoding for cellular fating RBPs with greater
210 expression in schizonts (**Fig. 3C, left panel**; **Table S3**). Notably, we identified eukaryotic translational
211 initiation factors (PVP01_1238100, PVP01_0531200, PVP01_1431600, PVP01_0807600,
212 PVP01_1005600, PVP01_0519700, PVP01_1329200, PVP01_0825000, PVP01_1303500), and
213 splicing factors (PVP01_0716000, PVP01_0521000, PVP01_0804100, PVP01_1111800,
214 PVP01_0607600, PVP01_1012200) suggesting active translational events. Gene Ontology (GO) term
215 analysis revealed that these transcripts were associated with translation initiation (GO:0005852;
216 GO:0033290; GO:0016282) (adjusted p value $< 0.05$, **Fig. 3C**; **Table S4**).

217 In hypnozoites, we detected 51 genes encoding for cellular fating RBPs with increased
218 expression relative to schizonts (**Fig. 3C**; **Table S3**). These transcripts encode for prominent P body
219 markers, namely DOZI/DDX6 (PVP01_0819400), CCR4-NOT complex proteins (PVP01_1429000,
220 PVP01_1014400, PVP01_1331700, PVP01_1453400, PVP01_0929400), mRNA-decapping enzyme
221 subunit 1 (PVP01_0617200), mRNA-decapping enzyme subunit 2 (PVP01_1409900), UPF1
222 (PVP01_0805200), UPF2 (PVP01_0724300), UPF3 (PVP01_1226700), PUF2 (PVP01_0526500),
223 PABP (PVP01_1442500), Fibrillarin (PVP01_1341600) and trailer hitch homolog (PVP01_1269800)
224 (**Table S3**). GO enrichment analysis of these transcripts encoding for cellular fating RBPs in hypnozoite
225 also represented GO terms corresponding to active biological condensate formations, such as the CCR4-
226 NOT complex (GO:0030014; GO:0030015) and the P body (GO:0000932) (adjusted p value < 0.05,
227 **Fig. 3C, right panel; Table S4**). Together, these findings suggest that P body-mediated cell fating could
228 be important in regulating hypnozoite persistence.

229 **Transcriptomic heterogeneity exists amongst individual *P. vivax* hypnozoites**

230 Having described the transcriptomic signatures distinguishing schizonts and hypnozoites, we next
231 sought to assess the extent to which gene expression varied amongst hypnozoites. We thus parsed the
232 data into only hypnozoite transcriptomes. In total, 1,147 transcriptomes were assessed (**Fig. 4A, left**
233 **panel**). Low dimensional representation of the data revealed slight variation between samples collected
234 at days 5 and 9 post-infection (**Fig. 4A, right panel**). After regrouping the data using the same
235 unsupervised clustering algorithm described previously, we identified three clusters (**Fig. 4B, right**
236 **panel**). The proportion of hypnozoites in each cluster varied across the day of collection: specifically,
237 the proportion of hypnozoites in cluster 3 (C3) was greater in hypnozoites collected at day 9 compared
238 to day 5 post-infection (**Fig. 4B, left panel; Fig. S4A**). Notably, we also found greater gene expression
239 of LISP2 in C3 relative to the other two clusters (**Fig. 4C**).

240 We next identified markers that define the hypnozoite in each cluster using the FindAllMarkers
241 function in Seurat (Stuart et al., 2019). We defined a marker as a transcript displaying greater than 0.5
242 FC (average $\log_2$) compared to the other clusters. In total, we detected 421 markers (adjusted p value <
243 0.05) (**Fig. S4B**; **Table S5**). Notable markers in C1 included transcripts associated with drug resistance
244 (PVP01_1447300, PVP01_1259100, and PVP01_1010900), energy metabolism (PVP01_1435000 and
245 PVP01_1122800), protein modification (PVP01_1248900 and PVP01_0916200), and RNA-binding
246 proteins (PVP01_0939900 and PVP01_0819400); in C2 those associated with translation
247 (PVP01_1255500 and PVP01_0822500); and in C3 those associated with translation (PVP01_0213700
248 and PVP01_0203400), fatty acid metabolism (PVP01_1143000 and PVP01_1022800), protein
249 processing (PVP01_1308000 and PVP01_0927700) and ion transport (PVP01_1407500) (**Fig. 4D**;
250 **Table S5**).

251 We next explored the data in the context of cellular fating to elucidate potential patterns in RBP
252 signatures. Among the hypnozoite markers found within our sub-clustering analysis, we identified 68
253 cellular fating RBPs, of which 54 RBPs were differentially expressed in at least in one of the three
254 clusters (adjusted p value < 0.05) (**Fig. 4E, top; Table S6**). Approximately 4% (2/54) of the
255 differentially expressed genes in C3 encoded for cellular fating. In this cluster, the increased gene
256 expression of eukaryotic translation initiation factor 4E (PVP01_0203400) further suggests active
257 translation events may be occurring. C2 contained ~16% (9/54) of the cellular fating RBPs differentially
258 expressed. In this cluster, we found RBPs which are important determinants of cell proliferation from a
259 state of senescence such as eukaryotic translation initiation factor 5A (PVP01_1303500),
260 polypyrimidine tract binding protein (PVP01_1142400), GTP-binding nuclear protein RAN/TC4
261 (PVP01_0918300), transformer-2 protein homolog beta (PVP01_0802200). C1 contained the majority
262 of the differentially expressed RBPs (~80%, 43/54). Within this cluster, we identified prominent P body
263 markers with cellular fating ability, such as DOZI/DDX6 (PVP01_0819400), CCR4-NOT complex
264 proteins (PVP01_1429000, PVP01_1014400, PVP01_1331700, PVP01_1453400), UPF1
265 (PVP01_0805200), UPF2 (PVP01_0724300), PABP (PVP01_1442500), Fibrillarin (PVP01_1341600)
266 and trailer hitch homolog (PVP01_1269800). GO analysis revealed enrichment of cellular
267 compartments associated to biological condensate formations, namely CCR4-NOT complex
268 (GO:0030014), P granule (GO:0043186), and germplasm (GO:0060293) (**Fig. 4E; Table S9**).

269 These findings, combined with the shift of hypnozoite proportions and increased transcript
270 levels of LISP2 from C1 to C3, allowed us infer the phenotype of hypnozoites in these clusters. As these
271 observations likely represent populations of hypnozoites in persisting and activating states, we defined
272 clusters C1, C2, and C3 to represent persisting, transitioning, and activating hypnozoites, respectively.
273 Together, these findings further our understanding of *P. vivax* hypnozoites through characterization of
274 gene usage and regulatory mechanisms in activating and persister forms. Furthermore, they highlight a
275 potential role of P body-mediated cellular fating governing persister hypnozoites.

276 **Strategy used to assess hepatocytes infected with *P. vivax* parasites**

277 After deciphering the identities of *P. vivax* transcriptomes representing schizonts and hypnozoites, we
278 next sought to characterize the transcriptional signatures of hepatocytes infected with either of these
279 forms. To this end, we integrated the data across all the conditions (**Figs. S5A and 5B)** and examined
280 whether distinct sub-populations of infected hepatocytes existed. As highlighted by the low dimensional
281 visualization of the data, we did not find a prominent pattern of infection (**Fig. 5A**). Moreover, we
282 detected parasites in hepatocytes with different metabolic states (MacParland et al., 2018), as
283 represented by their transcriptional signatures associated with different hepatocyte zonation programs
284 (**Figs. S5C and S5D**).

285 **Identification of transcriptional signatures in *P. vivax*-infected hepatocytes**

286 To identify host transcriptional signatures specific to infection status, we performed differential gene
287 expression analysis, comparing infected to non-infected hepatocytes. Among the hepatocytes infected
288 with schizonts, 106 hepatocyte transcripts displayed greater expression and 16 displayed decreased
289 expression; while in hepatocytes infected with hypnozoites, 365 genes displayed greater expression and
290 41 genes displayed decreased expression (adjusted p value < 0.05) (**Tables S10 and S11**). As depicted
291 in the volcano plots in **Fig. 6A**, the magnitude of change in expression in the infected versus non-infected
292 cells (average $\log_2$ fold change) was greater in hepatocytes containing schizonts compared to those
293 containing hypnozoites.

294 To gain greater insights into the biological processes and pathways that characterize a schizont-
295 or hypnozoite-infected hepatocyte, we performed enrichment analysis (Raudvere et al., 2019)—scoring
296 18,594 gene sets against the genes differentially expressed in each of our transcriptional comparisons.
297 When considering both the schizont- and hypnozoite-infected hepatocyte populations, we detected a
298 total of 254 enriched gene sets (adjusted p value < 0.05) (**Fig. 6B**; **Tables S8 and S9**). Approximately
299 18% (45/254) of these gene sets overlapped in hepatocytes infected with either schizonts or hypnozoites
300 (**Fig. S6; Table S11**). These data indicate that while some overlap exists in the gene networks the
301 parasite alters during infection, the majority of processes and pathways altered are specific to schizont
302 versus hypnozoite infected hepatocytes.

303 Using these gene sets, we then constructed network enrichment maps (Merico et al., 2010) to
304 provide a global overview of the prominent biological themes associated with each infection condition
305 (**Figs. 6C and 6D**). We detected upregulation of genes associated with pathways related to energy
306 metabolism (oxidative phosphorylation, mitochondrial function, and lipid catabolism) in schizont- and
307 hypnozoite-infected hepatocytes. Analysis of the most differentially expressed genes associated with
308 these pathways included *MT-ND2*, *CHCHD10*, and *AKR1B10* (**Tables S8 and S9**). Corroborating our
309 transcriptomic data, we found an increase in protein levels of AKR1B10 in infected versus non-infected
310 hepatocytes (**Figs. S6A-D**). AKR1B10 has been implicated in cell survival through its regulation of lipid
311 metabolism and elimination of carbonyls (Martin and Maser, 2009; Qu et al., 2021; Wang et al., 2009)
312 and has primarily been described as a biomarker of cancer (Díez-Dacal et al., 2011; Fukumoto et al.,
313 2005; Jin et al., 2006). More recently, it has been shown that its expression is positively correlated with
314 non-alcoholic fatty liver disease (Govaere et al., 2020). Its role during *Plasmodium* spp. liver stage
315 infection warrants further research. In schizonts, the upregulation of transcript linked to fatty acid
316 metabolism is consistent with observations in hepatocytes harboring developing forms from non-
317 relapsing Plasmodium spp. (Albuquerque et al., 2009; Itoe et al., 2014). We now reveal that infection

318 with hypnozoites also elicits enrichment of transcripts associated with fatty metabolism (**Fig. 6D**),
319 suggesting that these forms may be scavenging host resources to fuel their persistence.

320 Previous work assessing *Plasmodium* liver stage biology has revealed that the host is able to
321 detect the parasite (Liehl and Mota, 2012) and that type I interferon plays an integral role in this response
322 (Liehl et al., 2013; Miller et al., 2014). The decrease in transcripts associated with interferon signaling
323 (REAC:R-HSA-913531, GO:0034340, GO:0034341, GO:0071357, GO:0060337) in hepatocytes
324 infected with either schizonts or hypnozoites forms suggest that *P. vivax* manipulates the hepatocytes to
325 evade detection (**Figs. 6C and 6D; Table S10**). In hepatocytes infected with schizonts, we found a
326 decrease in expression of NFKB-regulated genes (*SOD2, TMEM45A, CCL20, and TPM1*) (**Table S8**),
327 consistent with findings that *Plasmodium* spp. release signals to block proinflammatory response (Singh
328 et al., 2007). These findings, in addition to the decrease in the expression of *HLA-B*—a molecule
329 involved in antigen presentation to T cells that can trigger their activation when 'self' peptides are not
330 presented—and the neutrophil chemoattractant *CXCL8* suggest that replicating parasites alter
331 hepatocyte signaling pathways to minimize recruitment of innate immune cells and avoid detection by
332 T cells.

333 Similar to hepatocytes infected with schizonts, we found transcripts associated with interferon
334 signaling downregulated in hepatocytes infected with hypnozoites, namely: *UBB, UBC, HSP90AB1,*
335 *IFITM3, IFITM2,* and *HLA-A* (**Table S9**). Furthermore, transcripts associated with the downregulation
336 of class major histocompatibility complex (*CD81* and *B2M*) were also decreased in these hepatocytes
337 (**Table S9**). Together, these findings suggest that *P. vivax* infection of hepatocytes may suppress the
338 secretion of various chemokines and proinflammatory cytokines to thwart the recruitment of
339 inflammatory cells to the site of infection while simultaneously reducing the chances they will be
340 detected if these cells are recruited by downregulating MHC- I.

341 Enrichment analysis linking the changes in gene expression in infected hepatocytes with
342 transcriptional factors revealed distinct sets of transcriptional regulators. In total, we detected 35
343 transcription factors with potential roles in governing the gene expression changes in infected
344 hepatocytes (adjusted p value < 0. 05, **Fig. 7A; Table S12**). In infected hepatocytes, we found
345 enrichment of transcripts governed by NRF2 (**Fig. 7A; Table S12)**. The regulation of gene expression
346 through NRF2 in infected hepatocytes may serve to minimize reactive oxygen species in the cell (Hayes
347 and Dinkova-Kostova, 2014). Thus, in addition to the decreased gene expression associated with
348 inflammatory response (**Table S10**), NRF2-mediated regulation of antioxidant responsive genes may
349 protect hepatocytes from *Plasmodium*-induced stress and thus serve as a complementary means of
350 minimizing the host inflammatory response.

351 **DISCUSSION**

352 The infection of the liver by *P. vivax* constitutes an obligatory step in its life-cycle. *In vivo* studies have
353 shown that within hepatocytes, *P. vivax* can exist in one of two phenotypically distinct forms: schizonts
354 or hypnozoites (Cogswell, 1992; Mikolajczak et al., 2015). They have also been observed *ex vivo* by
355 infection of hepatocyte monolayers (Gural et al., 2018; Hollingdale et al., 1985; Roth et al., 2018;
356 Sattabongkot et al., 2006). A key problem hindering the study of *P. vivax* liver stage biology is the
357 difficulty involved in obtaining a sufficient number of infected hepatocytes to make meaningful
358 comparisons between them. We show that by coupling our *in vitro* liver stage model (Maher et al., 2021;
359 Roth et al., 2018) with a high throughput single-cell capture technology (Klein et al., 2015; Macosko et
360 al., 2015; Zheng et al., 2017) transcriptome-wide characterization of a large number of infected
361 hepatocytes is feasible. Our approach therefore provides much needed insight into the molecular
362 signatures of *P. vivax* hypnozoites and the host cells they infect.

363 First, we found clear transcriptional differences between schizonts and hypnozoites. Our
364 transcriptome-wide assessment supports the notion that hypnozoites are metabolically active (Adams
365 and Mueller, 2017), demonstrated by the transcription associated with glycolysis and fatty acid
366 metabolism. Second, we found that hypnozoites exist in various transcriptomic states. We speculate that
367 these differences might represent a spectrum of phenotypes, from persisting to activating. The
368 differential expression of genes encoding for cellular fating RBPs supports the notion that these forms
369 may use post-transcriptional mechanisms to control gene usage (Mueller et al., 2019). The biological
370 significance of the enrichment of transcripts associated with translational repression, found exclusively
371 in a subpopulation of hypnozoites, suggests that this mechanism inhibits activation, and warrants further
372 investigation.

373 Second, we found distinct transcriptomic signatures of infected versus non-infected
374 hepatocytes, and showed that signalling pathways associated with energy metabolism, antioxidant
375 stress, and immune response are altered in infected hepatocytes. We found no clear pattern of infection,
376 as both schizonts and hypnozoites are detected in hepatocytes with various metabolic signatures. The
377 extent to which individual hepatocytes respond to *P. vivax* schizonts and hypnozoites has previously
378 been unknown. A bulk RNA sequencing approach has been used to identify pathways altered in
379 hepatocytes in response to *Plasmodium* infection (LaMonte et al., 2019); however, it is limited insofar
380 as it averages gene expression from millions of cells, obscuring any parasite-specific effects on the
381 infected cell. Targeted approaches have revealed that *P. vivax* liver forms recruit host factors to facilitate
382 growth (LaMonte et al., 2019; Posfai et al., 2020), but how certain infected hepatocyte populations
383 contribute to disease transmission, and how hepatocyte subpopulations support development, are
384 intriguing topics for future studies (Vijayan et al., 2021). Our data identify potential host factors

385 essential for *P. vivax*'s successful liver stage development. Whether certain hepatocyte phenotypes
386 influence the development, especially activation of hypnozoites into schizonts, requires further
387 investigation.

388 Several observations suggest protein degradation may be important for the parasite's liver
389 stages. Targeting this process may be an effective means of killing these forms. The ability of
390 hepatocytes to uptake and break down hemoglobin (Bissell et al., 1972) supports that this protein
391 substrate could be an essential amino acid source for the parasite. Our data suggest that several
392 mechanisms may allow *P. vivax* to utilize the amino acids derived from this protein. In hypnozoites, the
393 increased expression of genes encoding for proteases, such as vivapains, supports the idea that these
394 parasites digest host cytosolic proteins**.** The role of these proteins as hemoglobinases have been defined
395 extensively in *P. falciparum* blood stages (Drew et al., 2008; Rosenthal, 2011; Salas et al., 1995). A
396 similar role has been described for *P. vivax* (Byoung-Kuk et al., 2004), but there is limited information
397 about their significance in the liver stages. Vivapains are highly homologous to cathepsin protease L
398 (TgCpl) in the related apicomplexan *Toxoplasma gondii.* In these parasites, TgCpl is localized to its
399 plant-like vacuolar compartment—a lysosome-like organelle containing a variety of proteases (Parussini
400 et al., 2010)—and one of its functions is to aid in the digestion of host-derived proteins (Dou et al.,
401 2014). Genetic or chemical disruption of TgCpl negatively impacts the viability of bradyzoites, a
402 persisting form of this parasite (di Cristina et al., 2017). Given these orthologous proteins' roles in *P.*
403 *falciparum* and *T. gondii*, we speculate that the expression of vivapains may support the persistence of
404 *P. vivax* hypnozoites.

405 Persistence of hypnozoites is contingent on the longevity of the hepatocyte in which it resides.
406 The increased expression of genes associated with antioxidant stress (Scarpulla, 2002) is consistent with
407 the notion that hypnozoite infection induces changes in the hepatocyte to promote cell survival, in which
408 NRF-2 could be playing a regulatory role. We detected genes displaying greater expression in infected
409 hepatocytes related to NYFB-regulation, a transcription factor important for cell proliferation,
410 mitochondrial integrity, and cellular longevity (Tharyan et al., 2020). The increased expression of
411 mitochondria-related genes in hepatocytes infected with schizonts may be required to meet the parasite's
412 energy demands during replication, but the enrichment of mitochondria-related transcripts in cells
413 infected with hypnozoites could also aid in ensuring longevity of the hepatocyte. In addition to these
414 positive regulators of cell survival, we found negative regulation of transcripts through the decreased
415 expression of genes associated with cell death (*UBB, UBC,* and *HSP90AB1*). Their expression is thought
416 to be regulated by CEBPD, a transcription factor that has a role in governing cell death (Tsai et al., 2017;
417 Wang et al., 2019).

418 Persistence of hypnozoites also requires evading host detection, but how they are able to do so
419 has been elusive. Our analyses indicate that the parasite alters the host hepatocyte to evade detection by
420 immune cells. First, there is a decrease in expression of genes encoding for chemoattractants (*CCL20,*
421 *CXCL8, IL32*) in infected hepatocytes, and an increase in expression of PTGR1, a negative regulator of
422 the chemotactic factor leukotriene B4 (Yokomizo et al., 1993). These changes would result in decreased
423 secretion of chemokines that recruit innate immune cells to the liver, thereby reducing recruitment of
424 adaptive immune cells like CD8 T-cells that kill infected hepatocytes (Chakravarty et al., 2007).
425 Interestingly, there was also a decrease in expression of MHC-1 molecule (*HLA-A and -B*). The
426 presentation of parasite peptides to be detected by surveying CD8 T-cells would therefore be reduced
427 (Neefjes et al., 2011), creating an additional layer of protection should innate immune cells begin to be
428 recruited, for example upon lysis of the hepatocyte by schizonts. We propose that *P. vivax* infected
429 hepatocytes are re-programmed to prevent recruitment of innate immune cells on the one hand, and to
430 reduce the likelihood of their detection by the adaptive immune system on the other, all to enable
431 progress through schizogony and for hypnozoites to persist undetected. Understanding the mechanisms
432 leading up to this should be studied in the future, as their reversal may lead to improved clearance of
433 hypnozoites, thus reducing relapses. Indeed, a vaccine would need to decrease relapses to have any
434 impact on *P. vivax* transmission and disease (White et al., 2017). However, the decrease of MHC-I
435 expression in infected hepatocytes may mean that standard focuses to generate CD8 and CD4
436 polyfunctional T-cells in the liver may not be effective in eliminating *P. vivax* or other relapsing
437 parasites. Recent attempts to test anti-relapse vaccine candidates with *P. cynomolgi* did not prevent
438 relapses despite higher inducing IFNγ producing cells, a common metric used as a correlate of protection
439 (Kim et al., 2020), indicating that alternative strategies may be needed.

440 Our transcriptome-wide characterization of schizonts, hypnozoites, and the infected hepatocytes
441 highlights transcripts altered during infection, and provides a framework for examining the role of
442 infection dynamics of *P. vivax* liver stage infections. By examining two early liver stage time points at
443 single-cell resolution, our study lays out proof of principle and a technical advance demonstrating the
444 importance of *in vitro* models to shed light on the molecular basis of *P. vivax* liver stage development
445 and infection.

## 446 CONCLUSIONS

447 The overall aim of our research was to elucidate the molecular signatures of *P. vivax* liver infection, a
448 better understanding of which will aid in facilitating the development of new therapeutics to ultimately
449 reduce transmission. We anticipate that interventions could involve parasite- and/or host- directed small
450 molecule therapies, two approaches our group is actively pursuing. The comprehensive mapping of the

451 transcriptional landscape of both the host and *P. vivax* described here provides an important framework
452 for further investigation.

## 453 MATERIALS AND METHODS

### 454 Ethics statement

455 All research procedures were reviewed and approved by the Cambodian National Ethics Committee for
456 Health Research (approval numbers: #113NECHR, #104NECHR and #089NECHR).

### 457 Blood samples, mosquitos, and infections

458 The complete protocol used for mosquito rearing an infection has been published (Maher et al., 2021).
459 In brief, blood samples from symptomatic patients infected with *P. vivax* were collected at local health
460 facilities in Mondulkiri province in Cambodia from March 2020 to October 2021. Following a *P. vivax*
461 gametocyte-containing blood meal, *An. dirus* mosquitoes were maintained at ambient temperature on a
462 12:12 light: dark cycle and fed 10% sucrose + 0.5% PABA solution. *An. dirus* found positive for *P.*
463 *vivax* oocysts at six-days post-feeding were transported to the Institut Pasteur Cambodia Insectary
464 Facility in Phnom Penh, Cambodia where they were maintained under the same conditions described
465 above.

### 466 Sporozoite isolation and primary human hepatocyte infections

467 The complete protocol used for seeding primary human hepatocytes, harvesting sporozoites, and
468 infecting cultures has been published (Maher et al., 2021). In brief, *P. vivax* sporozoites were isolated
469 from the salivary glands of female *An. dirus* mosquitoes 18 days after an infectious blood-meal. Primary
470 human hepatocytes (Lot BGW, BioIVT) were seeded 2 days before infection with 30,000 sporozoites
471 (replicate 1), or 15,200 sporozoites (replicate 2) per well. Media was replaced with fresh CP media
472 (BioIVT) containing antibiotics (penicillin, streptomycin, and gentamycin) the day after infection and
473 every 2-3 days thereafter. Hepatocytes containing solely hypnozoites at 9 days post-infection were
474 treated with 1 µM MMV390048 on days 5, 6, and 7 post-infection to kill replicating schizonts. At days
475 5 and 9 post-infection, cultures were processed for single-cell sorting (described in the following
476 section) or immunofluorescence assay (IFA). For the latter, hepatocytes were fixed with 4%
477 paraformaldehyde in 1X PBS. Fixed cultures were then stained overnight at 4ºC with recombinant
478 mouse anti-*P. vivax* UIS4 antibody (Schäfer et al., 2018) diluted 1:25,000 in a stain buffer (0.03% Triton
479 X-100 and 1% (w/v) BSA in 1X PBS. The following day, cultures were washed three times with 1X
480 PBS and then stained overnight at 4ºC with 1:1,000 rabbit anti-mouse AlexaFluor ™488-conjugated

481 antibody diluted 1:1,000 in stain buffer. Cultures were washed three times with 1X PBS and
482 counterstained with 1 mg/mL Hoechst 33342 (Thermo Fisher) to detect parasite and host DNA. High
483 content imaging was performed on a Lionheart imaging system (Biotek). Quantification of the number
484 of nuclei and parasite liver forms was performed using Gen5 high content analysis software (Biotek).
485 Confocal images were obtained using an ImageXpress Micro (Molecular Devices).

486 **Single-cell partitioning, library preparation, and sequencing**

487 Hepatocyte cultures infected with *P. vivax* were processed prior to- and post- PI4K treatment (5- and 9-
488 days post-infection, respectively). Two replicate experiments, defined as an independent plating of
489 hepatocytes infected with sporozoites from a unique field isolate, were performed several months apart.
490 Additionally, and as a negative control, one replicate of hepatocyte cultures never exposed to *P. vivax*
491 (naïve) were processed similarly to those that were infected. At each endpoint for each replicate,
492 approximately 640,000 PHH hepatocytes (16 wells of a 384-well plate each having approximately
493 10,000 cells) were treated with trypsin (Corning 25-053-Cl) to facilitate their detachment from the plate.
494 Once detached, trypsin was inactivated with 1:1 complete media and the cell suspension was collected
495 into a 5mL protein-low bind centrifuge tube (Eppendorf). To remove residual trypsin, hepatocytes were
496 washed via three sequential rounds of pelleting (50 x g, 3 min, 4ºC) and resuspending in 1X PBS
497 containing 0.1% BSA. Cells were then passed through a 35µm strainer (Falcon 352235) to minimize or
498 remove hepatocyte clusters. Prior to partitioning cells on the Chromium controller (10x Genomics),
499 hepatocytes were counted and the cell concentration was assessed using a hemocytometer.
500 Approximately 10,000 hepatocytes were loaded on a Chromium Chip B (10x Genomics) as per
501 manufacturer's recommendations. Chips containing hepatocyte suspensions, Gel Beads in Emulsion
502 (GEMs), and reverse transcription reagents were loaded into the Chromium controller (10x Genomics)
503 for single-cell partitioning and cell barcoding. Barcoded cDNA libraries were generated according to
504 the Chromium Single Cell 3' gene expression protocol (version 3). In total, 6 cDNA libraries were
505 generated (two replicates at 5 days post-infection, two replicates at 9 days post-infection, one uninfected
506 control for day 5 cultures, and one uninfected control for day 9 cultures). Libraries were loaded on
507 individual flow cell lanes and sequenced at a depth of 400 million reads using a HiSeq X Ten platform
508 (Illumina) at Macrogen (Seoul, Korea).

509 **Computational analysis of single-cell RNA sequencing data**

510 Quality control checks on the raw sequencing data were performed using FASTQC (Andrews, 2010). A
511 multi-species transcriptome index—containing the transcriptomes for *P. vivax* P01 (PlasmoDB.org,
512 version 51) and *H. sapiens* GRCh8 (Ensembl version 103)—was created using the 'ref' function in kb-
513 python (0.26.3) (Bray et al., 2016; Melsted et al., 2021). Next, reads pseudoaligned and counted using

514 the ‘count’ function in kb-python with default parameters selected. The resulting unfiltered cell-gene
515 count matrices were read into R (v 4.1.1) for further processing.

516 **Filtering and normalization of scRNA-seq count matrices**

517 R scripts containing all computational analyses will be available on a dedicated GitHub repository upon
518 publication.

519 To distinguish between droplets containing cells and those only with ambient RNA, we used
520 emptyDrops function (Lun et al., 2019) with the lower total UMI count threshold (at or below which all
521 barcodes are assumed to correspond to empty droplets) set to 1,000. The droplets with cells (FDR <
522 0.001), more specifically, those containing barcoded transcripts derived from either human, parasite, or
523 a combination of the two—were kept for downstream processing.

524 **Assessment of *P. vivax* liver stage transcriptomes**

525 For the analyses of *P. vivax*, we filtered out the transcripts derived from human, leaving only transcripts
526 derived from the parasite quantifiable. For each sample, cells with less than 200 UMIs were removed.
527 Next, we filtered out low detected genes, retaining transcripts with 10 or greater UMIs. Post cell and
528 gene filtering, the data were normalized using Seurat (Stuart et al., 2019) ‘LogNormalize’ function with
529 the default parameters selected.

530 *Data integration and clustering*

531 The data were integrated using Seurat’s SCTransform function (Hafemeister and Satija, 2019)
532 with the following parameters indicated: variable.features.n = NULL, variable.features.rv.th = 1.3.
533 Clustering was performed using Seurat’s SNN-Leiden algorithm (Traag et al., 2019). The full
534 description of this analysis is found in the extended methods.

535 *Differential gene expression analysis*

536 To detect differentially expressed transcripts, the Seurat function FinalAllMarkers and
537 FindMarkers were used. For differential gene expression testing using the FindMarkers function, we
538 used the following parameters: logfc.threshold = 0.0, ident.1 = '1', ident.2 = '2', test.use = "wilcox",
539 min.pct = 0, only.pos = F, assay = "RNA". For differential gene expression testing using the
540 FindAllMarkers function, we used the following parameters: test.use = "wilcox", only.pos = T, assay =
541 "RNA", log2FC = 0.0.

542 *RBP analyses*

543 RBPs with cell fating potential reported in humans (Decker and Parker; Gerstberger et al., 2014;
544 Guallar and Wang, 2014; Voronina et al., 2011; Youn et al., 2019) were manually curated. The
545 orthologue's counterparts of these cell fating RBPs from the *P. vivax* PVP01 genome were mined using
546 OrthoMCL (Release-6.8)(Chen et al., 2006). Within the differentially expressed genes in *P. vivax*,
547 transcripts encoding for cell fating RBPs were filtered for further assessment.

548 *GO enrichment analyses*

549 GO enrichment analysis was performed on the PlasmoDB (v55) website with the following
550 input parameters selected: P value cutoff = 0.05; Limit to GO Slim terms = No; Evidence: Computed,
551 curated. Enrichment from GO cellular compartment (CC), biological processes (BP), and molecular
552 function (MF) were all assessed.

553 **Assessment of host hepatocyte transcriptomes**

554 For the analyses of the host, we removed all transcripts derived from *P. vivax*, leaving only the
555 transcripts derived from hepatocytes. We retained transcripts detected in at least 30 cells. Next, cells
556 with less than 1,500 UMIs were removed from further analyses**.** Post-cell and gene filtering, the data
557 from each replicate were normalized using Seurat's 'LogNormalize' function with the default
558 parameters.

559 *Data integration and clustering*

560 Filtered, normalized data matrices were integrated in a manner described in in the Seurat
561 (version 4) vignette, *Introduction to scRNA-seq integration*, available on the Sajita Lab's website
562 (https://satijalab.org/seurat/articles/integration_introduction.html). Briefly, integration features were
563 identified in each replicate using the 'SelectIntegrationFeatures' function. Next, integration anchors
564 were identified using the 'FindIntegrationAnchors'. Last, using these anchors, the four datasets were
565 integrated using the 'IntegrateData' function. Clustering was performed using Seurat's SNN-Leiden
566 algorithm (Traag et al., 2019).

567 *Gene Ontology and Reactome enrichment analyses*

568 Enriched biological processes and pathways were determined using gProfiler (Raudvere et al.,
569 2019) with the following options selected: ordered query, statistical domain scope—only annotated
570 genes, significance threshold—g:SCS threshold, user threshold—0.05, Gene Ontology—GO biological
571 processes, No electronic GO annotations, biological pathways—Reactome. Transcripts that displayed

572 significant changes in expression in infected hepatocytes versus non-infected hepatocytes were used as
573 input. EnrichmentMap (v 1.1.0) (Merico et al., 2010) for CytoScape (v 3.8.2) (Shannon et al., 2003) was
574 used to create the enrichment networks. Significantly enriched GO biological processes and Reactome
575 pathways (adjusted p value < 0.05) were used as input. Pathways were clustered and annotated using
576 the AutoAnnotate function (Kucera et al., 2016). Node size corresponds to the number of transcripts in
577 the corresponding set, and edge widths correspond to the number of transcripts shared between sets.

578 *Transcription factor enrichment analysis*

579 We downloaded curated sets of known transcription factors from the website
580 (http://amp.pharm.mssm.edu/Enrichr/). Transcription factor—target gene sets were obtained by ChIP-
581 X experiments from the ChEA (Lachmann et al., 2010) and ENCODE (Feingold et al., 2004) projects.
582 TF-target relationships using Chip-seq data from ENCODE and CHEA were used to identify
583 overrepresented pathways and TFs. Differentially expressed genes (adjusted p value < 0.05) in each
584 condition versus non-infected cells were used as inputs. Gene sets with an adjusted p value < 0.05 were
585 considered significantly enriched.

586 **Carfilzomib dose-response assessment**

587 A carfilzomib dose-response against *P. vivax* liver forms was obtained from three independent
588 experiments, in which a different *P. vivax* clinical isolate was allowed to infect BGW human
589 hepatocytes. The 12-day assay was used (Maher et al., 2021). All independent experiments resulted in
590 sufficient hypnozoite formation within each well for dose-response calculations. Liver stage parasite
591 growth metrics and compound dilutions were loaded into CDD Vault (Collaborative Drug Discovery)
592 and growth data normalized such that zero (negative) inhibition was set as the average of DMSO wells
593 and 100% (positive) inhibition was set to the effective doses of a nigericin control. Normalized values
594 were then combined in Graphpad Prism to fit a dose-response curve and calculated $IC_{50}$ values from all
595 replicates.

596 **Quantification of AKR1B10 protein expression**

597 To analyze AKR1B10 expression and localization, *P. vivax*-infected PHHs were fixed 12 days post-
598 infection. Infected wells were then permeabilized for 20 minutes with 0.2% TritonX-100, washed thrice
599 with 1X PBS, and blocked in 3% BSA for one hour. Primary antibodies rabbit anti-HsAKR1B10 (PA5-
600 30773, Thermo Fisher) and mouse anti-PvUIS4 were sequentially added, diluted 1:100 and 1:500,
601 respectively. Antibodies were incubated overnight at 4ºC and washed 3 times with 1X PBS before
602 addition of 1:400 Alexa- Fluor 568 donkey anti-rabbit for HsAKR1B10 or 1:400 AlexaFluor 488 goat

603 anti-mouse for PvUIS4. Secondary antibodies were incubated overnight at 4ºC. Cells were washed thrice
604 with 1X PBS before adding 0.5 mg/mL DAPI for 10 minutes. Cells were washed 3 final times with 1X
605 PBS before image collection with an ImageXpress inverted confocal microscope (Molecular Devices).
606 Image analysis was completed using MetaXpress analysis software (Molecular Devices).

607 **Contact for reagent and resource sharing**

608 Further information and requests for resources and reagents should be directed to and will be fulfilled
609 by the Lead Contact, Dennis Kyle (email: dennis.kyle@uga.edu).

610 **Data availability**

611 Raw sequencing files (FASTQ), processed data, scripts, and all host- and parasite- differentially
612 expressed genes will be made publicly available upon publication of the manuscript.

613 **Acknowledgements**

614 We thank the patients of Mondulkiri Province, Cambodia, for participating in this study. We thank the
615 Institut Pasteur du Cambodge's field site manager (Saorin Kim) for logistical assistance, insectary staff
616 (Makara Pring, Koeun Kaing, Nora Sambath) for the *An. dirus* mosquito colony maintenance, and
617 laboratory staff (Eakpor Piv, Chansophea Chhin, Sreyvouch Phen, Chansovandan Chhun, Sivcheng
618 Phal, Baura Tat) for assistance with the mosquito dissections and the *in vitro* assays.

619 High-content imaging data was produced in part by the Biomedical Microscopy Core at the
620 University of Georgia, supported by the Georgia Research Alliance. A.R.J., B.B. and I.M. acknowledge
621 support from the Victorian State Government Operational Infrastructure Support and Australian
622 Government National Health and Medical Research Council Independent Research Institute
623 Infrastructure Support Scheme. This work was also supported by the Agence Nationale de la Recherche
624 (ANR-17-CE13-0025 to A.A.R and I.M.); an Australian National Health and Medical Research Council
625 Leadership Fellowship (APP1194330 to A.R.J.); the Bill & Melinda Gates Foundation (OPP1023601
626 to D.E.K.); and Medicines for Malaria Venture (RD/2017/0042 to B.W. and A.V., RD/16/1082 and
627 RD/15/0022 to S.P.M. and D.E.K.).

628 A.A.R., S.P.M., A.V., I.M., B.W. and D.E.K conceived and designed the study; A.A.R, S.P.M.
629 and A.V. performed the experiments; A.A.R., C.B., B.B. and C.J. curated the data; A.A.R., S.P.M., B.B.,
630 A.R.J. and C.J. performed the formal analyses; S.P.M., A.V. and I.M., B.W. and D.E.K. coordinated the
631 research activities; S.P.M., A.V., I.M., B.W. and D.E.K. provided resources; S.P.M. and D.E.K.

632 acquired funding for the work; A.A.R wrote the initial draft of the article; all authors reviewed and made
633 contributions to the submitted article.

634 **REFERENCES**


635 Adams, J.H., and Mueller, I. (2017). The Biology of Plasmodium vivax. Cold Spring Harbor
636 Perspectives in Medicine *7*, a025585.

637 Adekunle, A.I., Pinkevych, M., McGready, R., Luxemburger, C., White, L.J., Nosten, F., Cromer, D.,
638 and Davenport, M.P. (2015). Modeling the Dynamics of Plasmodium vivax Infection and Hypnozoite
639 Reactivation In Vivo. PLOS Neglected Tropical Diseases *9*, e0003595.

640 Albuquerque, S.S., Carret, C., Grosso, A.R., Tarun, A.S., Peng, X., Kappe, S.H.I., Prudêncio, M., and
641 Mota, M.M. (2009). Host cell transcriptional profiling during malaria liver stage infection reveals a
642 coordinated and sequential set of biological events. BMC Genomics *10*, 1–13.

643 Aldridge, S., and Teichmann, S.A. (2020). Single cell transcriptomics comes of age. Nature
644 Communications 2020 11:1 *11*, 1–4.

645 Andrews, S. (2010). FastQC: A quality control tool for high throughput sequence data. Available at:
646 Http://Www.Bioinformatics.Babraham.Ac.Uk/Projects/Fastqc.

647 Balu, B., Maher, S.P., Pance, A., Chauhan, C., Naumov, A. v., Andrews, R.M., Ellis, P.D., Khan, S.M.,
648 Lin, J. wen, Janse, C.J., et al. (2011). CCR4-Associated Factor 1 Coordinates the Expression of
649 Plasmodium falciparum Egress and Invasion Proteins. Eukaryotic Cell *10*, 1257.

650 Battle, K.E., Karhunen, M.S., Bhatt, S., Gething, P.W., Howes, R.E., Golding, N., van Boeckel, T.P.,
651 Messina, J.P., Shanks, G.D., Smith, D.L., et al. (2014). Geographical variation in Plasmodium vivax
652 relapse. Malaria Journal *13*, 1–16.

653 Baumgarten, S., Bryant, J.M., Sinha, A., Reyser, T., Preiser, P.R., Dedon, P.C., and Scherf, A. (2019).
654 Transcriptome-wide dynamics of extensive m6A mRNA methylation during Plasmodium falciparum
655 blood-stage development. Nature Microbiology *4*, 2246.

656 Bissell, D.M., Hammaker, L., and Schmid, R. (1972). Hemoglobin and Erythrocyte Catabolism in Rat
657 Liver: The Separate Roles of Parenchymal and Sinusoidal Cells. Blood *40*, 812–822.

658 Bogale, H.N., Pascini, T. v., Kanatani, S., Sá, J.M., Wellems, T.E., Sinnis, P., Vega-Rodríguez, J., and
659 Serre, D. (2021). Transcriptional heterogeneity and tightly regulated changes in gene expression during
660 *Plasmodium berghei* sporozoite development. Proceedings of the National Academy of Sciences *118*,
661 e2023438118.

662 Bray, N.L., Pimentel, H., Melsted, P., and Pachter, L. (2016). Near-optimal probabilistic RNA-seq
663 quantification. Nature Biotechnology *34*, 525–527.

664 Bunnik, E.M., Batugedara, G., Saraf, A., Prudhomme, J., Florens, L., and le Roch, K.G. (2016). The
665 mRNA-bound proteome of the human malaria parasite Plasmodium falciparum. Genome Biology *17*.

666 Byoung-Kuk, N.A., Shenai, B.R., Sijwali, P.S., Choe, Y., Pandey, K.C., Singh, A., Craik, C.S., and
667 Rosenthal, P.J. (2004). Identification and biochemical characterization of vivapains, cysteine proteases
668 of the malaria parasite Plasmodium vivax. Biochemical Journal *378*, 529.

669 Caldelari, R., Dogga, S., Schmid, M.W., Franke-Fayard, B., Janse, C.J., Soldati-Favre, D., and Heussler,
670 V. (2019). Transcriptome analysis of Plasmodium berghei during exo-erythrocytic development.
671 Malaria Journal *18*, 330.

672 Chakravarty, S., Cockburn, I.A., Kuk, S., Overstreet, M.G., Sacci, J.B., and Zavala, F. (2007). CD8+ T
673 lymphocytes protective against malaria liver stages are primed in skin-draining lymph nodes. Nature
674 Medicine 2007 13:9 *13*, 1035–1041.

675 Chen, F., Mackey, A.J., Stoeckert, C.J., and Roos, D.S. (2006). OrthoMCL-DB: querying a
676 comprehensive multi-species collection of ortholog groups. Nucleic Acids Research *34*.

677 Chua, A.C.Y., Jie, J., Ong, Y., Malleret, B., Suwanarusk, R., Kosaisavee, V., Zeeman, A.-M., Cooper,
678 C.A., Tan, K.S.W., Zhang, R., et al. (2019). Robust continuous in vitro culture of the Plasmodium
679 cynomolgi erythrocytic stages. Nature Communications *10*, 1–13.

680 Cogswell, F.B. (1992). The hypnozoite and relapse in primate malaria. Clinical Microbiology Reviews
681 *5*, 26–35.

682 Commons, R.J., Simpson, J.A., Watson, J., White, N.J., and Price, R.N. (2020). Estimating the
683 Proportion of Plasmodium vivax Recurrences Caused by Relapse: A Systematic Review and Meta-
684 Analysis. The American Journal of Tropical Medicine and Hygiene *103*, 1094–1099.

685 di Cristina, M., Dou, Z., Lunghi, M., Kannan, G., Huynh, M.-H., McGovern, O.L., Schultz, T.L.,
686 Schultz, A.J., Miller, A.J., Hayes, B.M., et al. (2017). Toxoplasma depends on lysosomal consumption
687 of autophagosomes for persistent infection.

688 Cubi, R., Vembar, S.S., Biton, A., Franetich, J.-F., Bordessoulles, M., Sossau, D., Zanghi, G., Bosson-
689 Vanga, H., Benard, M., Moreno, A., et al. (2017). Laser capture microdissection enables transcriptomic
690 analysis of dividing and quiescent liver stages of Plasmodium relapsing species. Cellular Microbiology
691 *19*, e12735.

692 Dame, J.B., Yowell, C.A., Omara-Opyene, L., Carlton, J.M., Cooper, R.A., and Li, T. (2003).
693 Plasmepsin 4, the food vacuole aspartic proteinase found in all Plasmodium spp. infecting man.
694 Molecular and Biochemical Parasitology *130*, 1–12.

695 Decker, C.J., and Parker, R. P-Bodies and Stress Granules: Possible Roles in the Control of Translation
696 and mRNA Degradation.

697 Díez-Dacal, B., Gayarre, J., Gharbi, S., Timms, J.F., Coderch, C., Gago, F., and Pérez-Sala, D. (2011).
698 Identification of aldo-keto reductase AKR1B10 as a selective target for modification and inhibition by
699 prostaglandin A(1): implications for antitumoral activity. Cancer Research *71*, 4161–4171.

700 Dou, C., Mcgovern, Z.L., Cristina, D. di, and Carruthers, M.B. (2014). Toxoplasma gondii ingests and
701 digests host cytosolic proteins. MBio *5*, 1188–1202.

702 Drew, M.E., Banerjee, R., Uffman, E.W., Gilbertson, S., Rosenthal, P.J., and Goldberg, D.E. (2008).
703 Plasmodium Food Vacuole Plasmepsins Are Activated by Falcipains. The Journal of Biological
704 Chemistry *283*, 12870.

705 Feingold, E.A., Good, P.J., Guyer, M.S., Kamholz, S., Liefer, L., Wetterstrand, K., Collins, F.S.,
706 Gingeras, T.R., Kampa, D., Sekinger, E.A., et al. (2004). The ENCODE (ENCyclopedia of DNA
707 Elements) Project. Science *306*, 636–640.

708 Foth, B.J., Zhang, N., Chaal, B.K., Sze, S.K., Preiser, P.R., and Bozdech, Z. (2011). Quantitative time-
709 course profiling of parasite and host cell proteins in the human malaria parasite Plasmodium falciparum.
710 Molecular and Cellular Proteomics *10*.

711 Fukumoto, S.I., Yamauchi, N., Moriguchi, H., Hippo, Y., Watanabe, A., Shibahara, J., Taniguchi, H.,
712 Ishikawa, S., Ito, H., Yamamoto, S., et al. (2005). Overexpression of the aldo-keto reductase family

713 protein AKR1B10 is highly correlated with smokers' non-small cell lung carcinomas. Clinical Cancer
714 Research : An Official Journal of the American Association for Cancer Research *11*, 1776–1785.

715 Gerstberger, S., Hafner, M., and Tuschl, T. (2014). A census of human RNA-binding proteins. Nature
716 Reviews Genetics 2014 15:12 *15*, 829–845.

717 Govaere, O., Cockell, S., Tiniakos, D., Queen, R., Younes, R., Vacca, M., Alexander, L., Ravaioli, F.,
718 Palmer, J., Petta, S., et al. (2020). Transcriptomic profiling across the nonalcoholic fatty liver disease
719 spectrum reveals gene signatures for steatohepatitis and fibrosis. Science Translational Medicine *12*.

720 Guallar, D., and Wang, J. (2014). RNA-binding proteins in pluripotency, differentiation, and
721 reprogramming. Frontiers in Biology *9*, 389–409.

722 Gupta, D.K., Dembele, L., Voorberg-Van Der Wel, A., Roma, G., Yip, A., Chuenchob, V.,
723 Kangwanrangsan, N., Ishino, T., Vaughan, A.M., Kappe, S.H., et al. (2019). The plasmodium liver-
724 specific protein 2 (LISP2) is an early marker of liver stage development. ELife *8*.

725 Gural, N., Mancio-Silva, L., Miller, A.B., Galstian, A., Butty, V.L., Levine, S.S., Patrapuvich, R., Desai,
726 S.P., Mikolajczak, S.A., Kappe, S.H.I., et al. (2018). In Vitro Culture, Drug Sensitivity, and
727 Transcriptome of Plasmodium Vivax Hypnozoites. Cell Host & Microbe *23*, 395-406.e4.

728 Hafemeister, C., and Satija, R. (2019). Normalization and variance stabilization of single-cell RNA-seq
729 data using regularized negative binomial regression. Genome Biology *20*, 1–15.

730 Hayes, J.D., and Dinkova-Kostova, A.T. (2014). The Nrf2 regulatory network provides an interface
731 between redox and intermediary metabolism. Trends in Biochemical Sciences *39*, 199–218.

732 Hentze, M.W., Castello, A., Schwarzl, T., and Preiss, T. (2018). A brave new world of RNA-binding
733 proteins. Nature Reviews Molecular Cell Biology 2018 19:5 *19*, 327–341.

734 Hollingdale, M.R., Collins, W.E., Campbell, C., and Schwartz, A.L. (1985). In vitro culture of two
735 populations (dividing and nondividing) of exoerythrocytic parasites of Plasmodium vivax. The
736 American Journal of Tropical Medicine and Hygiene *34*, 216–222.

737 Howick, V.M., Russell, A.J.C., Andrews, T., Heaton, H., Reid, A.J., Natarajan, K., Butungi, H., Metcalf,
738 T., Verzier, L.H., Rayner, J.C., et al. (2019). The Malaria Cell Atlas: Single parasite transcriptomes
739 across the complete Plasmodium life cycle. Science (New York, N.Y.) *365*, eaaw2619.

740 Huldén, L., Huldén, L., and Heliövaara, K. (2008). Natural relapses in vivax malaria induced by
741 Anopheles mosquitoes. Malaria Journal *7*, 1–11.

742 Itoe, M.A., Sampaio, J.L., Cabal, G.G., Real, E., Zuzarte-Luis, V., March, S., Bhatia, S.N., Frischknecht,
743 F., Thiele, C., Shevchenko, A., et al. (2014). Host Cell Phosphatidylcholine Is a Key Mediator of Malaria
744 Parasite Survival during Liver Stage Infection. Cell Host & Microbe *16*, 778.

745 Jin, J., Krishack, P., and Cao, D. (2006). Role of aldo-keto reductases in development of prostate and
746 breast cancer. Frontiers in Bioscience : A Journal and Virtual Library *11*, 2767–2773.

747 Kim, Y.C., Dema, B., Rodriguez-Garcia, R., López-Camacho, C., Leoratti, F.M.S., Lall, A., Remarque,
748 E.J., Kocken, C.H.M., and Reyes-Sandoval, A. (2020). Evaluation of Chimpanzee Adenovirus and
749 MVA Expressing TRAP and CSP from Plasmodium cynomolgi to Prevent Malaria Relapse in
750 Nonhuman Primates. Vaccines *8*, 1–14.

751 Kivioja, T., Vähärautio, A., Karlsson, K., Bonke, M., Enge, M., Linnarsson, S., and Taipale, J. (2011).
752 Counting absolute numbers of molecules using unique molecular identifiers. Nature Methods *9*, 72–74.

753 Klein, A.M., Mazutis, L., Akartuna, I., Tallapragada, N., Veres, A., Li, V., Peshkin, L., Weitz, D.A.,
754 and Kirschner, M.W. (2015). Droplet barcoding for single-cell transcriptomics applied to embryonic
755 stem cells. Cell *161*, 1187–1201.

756 Kortuem, K.M., and Stewart, A.K. (2013). Carfilzomib. Blood *121*, 893–897.

757 Krotoski, W.A., Collins, W.E., Bray, R.S., Garnham, P.C., Cogswell, F.B., Gwadz, R.W., Killick-
758 Kendrick, R., Wolf, R., Sinden, R., Koontz, L.C., et al. (1982). Demonstration of hypnozoites in
759 sporozoite-transmitted Plasmodium vivax infection. The American Journal of Tropical Medicine and
760 Hygiene *31*, 1291–1293.

761 Krotoski, W.A., Garnham, P.C.C., Cogswell, F.B., Collins, W.E., Bray, R.S., Gwasz, R.W., Killick-
762 Kendrick, R., Wolf, R.H., Sinden, R., and Hollingdale, M. (1986). Observations on early and late post-
763 sporozoite tissue stages in primate malaria. IV. Pre-erythrocytic schizonts and/or hypnozoites of
764 Chesson and North Korean strains of Plasmodium vivax in the chimpanzee. American Journal of
765 Tropical Medicine and Hygiene *35*, 263–274.

766 Kucera, M., Isserlin, R., Arkhangorodsky, A., and Bader, G.D. (2016). AutoAnnotate: A Cytoscape app
767 for summarizing networks with semantic annotations. F1000Research *5*.

768 Lachmann, A., Xu, H., Krishnan, J., Berger, S.I., Mazloom, A.R., and Ma'ayan, A. (2010). ChEA:
769 transcription factor regulation inferred from integrating genome-wide ChIP-X experiments.
770 Bioinformatics (Oxford, England) *26*, 2438–2444.

771 LaMonte, G.M., Orjuela-Sanchez, P., Calla, J., Wang, L.T., Li, S., Swann, J., Cowell, A.N., Zou, B.Y.,
772 Abdel-Haleem Mohamed, A.M., Villa Galarce, Z.H., et al. (2019). Dual RNA-seq identifies human
773 mucosal immunity protein Mucin-13 as a hallmark of Plasmodium exoerythrocytic infection. Nature
774 Communications *10*, 488.

775 Liehl, P., and Mota, M.M. (2012). Innate recognition of malarial parasites by mammalian hosts.
776 International Journal for Parasitology *42*, 557–566.

777 Liehl, P., Zuzarte-Luís, V., Chan, J., Zillinger, T., Baptista, F., Carapau, D., Konert, M., Hanson, K.K.,
778 Carret, C., Lassnig, C., et al. (2013). Host-cell sensors for Plasmodium activate innate immunity against
779 liver-stage infection. Nature Medicine 2013 20:1 *20*, 47–53.

780 Lun, A.T.L., Riesenfeld, S., Andrews, T., Dao, T.P., Gomes, T., and Marioni, J.C. (2019). EmptyDrops:
781 distinguishing cells from empty droplets in droplet-based single-cell RNA sequencing data. Genome
782 Biology *20*, 63.

783 Lysenko Ja., A., Beljaev, A.E., and Rybalka, V.M. (1977). Population studies of Plasmodium vivax: 1.
784 The theory of polymorphism of sporozoites and epidemiological phenomena of tertian malaria. Bulletin
785 of the World Health Organization *55*, 541.

786 Macosko, E.Z., Basu, A., Satija, R., Nemesh, J., Shekhar, K., Goldman, M., Tirosh, I., Bialas, A.R.,
787 Kamitaki, N., Martersteck, E.M., et al. (2015). Highly Parallel Genome-wide Expression Profiling of
788 Individual Cells Using Nanoliter Droplets. Cell *161*, 1202–1214.

789 MacParland, S.A., Liu, J.C., Ma, X.-Z., Innes, B.T., Bartczak, A.M., Gage, B.K., Manuel, J., Khuu, N.,
790 Echeverri, J., Linares, I., et al. (2018). Single cell RNA sequencing of human liver reveals distinct
791 intrahepatic macrophage populations. Nature Communications *9*, 4383.

792 Maher, S., Vantaux, A., Cooper, C., Chasen, N., Cheng, W., Joyner, C., Manetsch, R., Witkowski, B.,
793 and Kyle, D. (2021). A Phenotypic Screen for the Liver Stages of Plasmodium vivax. BIO-PROTOCOL
794 *11*.

795 Mancio-Silva, L., Gural, N., Wadsworth, M.H., Butty, V.L., Hughes, T.K., March, S., Nerurkar, N.,
796 Roobsoong, W., Fleming, H.E., Whittaker, C., et al. (2021). Gene signatures and host-parasite
797 interactions revealed by dual single-cell profiling of Plasmodium vivax liver infection. BioRxiv
798 2021.09.01.454555.

799 Martin, H.J., and Maser, E. (2009). Role of human aldo–keto-reductase AKR1B10 in the protection
800 against toxic aldehydes. Chemico-Biological Interactions *178*, 145–150.

801 Melsted, P., Booeshaghi, A.S., Liu, L., Gao, F., Lu, L., Min, K.H. (Joseph), da Veiga Beltrame, E.,
802 Hjörleifsson, K.E., Gehring, J., and Pachter, L. (2021). Modular, efficient and constant-memory single-
803 cell RNA-seq preprocessing. Nature Biotechnology 2021 39:7 *39*, 813–818.

804 Merico, D., Isserlin, R., Stueker, O., Emili, A., and Bader, G.D. (2010). Enrichment Map: A Network-
805 Based Method for Gene-Set Enrichment Visualization and Interpretation. PLOS ONE *5*, e13984.

806 Miao, J., Li, J., Fan, Q., Li, X., Li, X., and Cui, L. (2010). The Puf-family RNA-binding protein PfPuf2
807 regulates sexual development and sex differentiation in the malaria parasite Plasmodium falciparum.
808 Journal of Cell Science *123*, 1039.

809 Mikolajczak, S.A., Vaughan, A.M., Kangwanrangsan, N., Roobsoong, W., Fishbaugher, M.,
810 Yimamnuaychok, N., Rezakhani, N., Lakshmanan, V., Singh, N., Kaushansky, A., et al. (2015).
811 Plasmodium vivax liver stage development and hypnozoite persistence in human liver-chimeric mice.
812 Cell Host & Microbe *17*, 526–535.

813 Miller, J.L., Sack, B.K., Baldwin, M., Vaughan, A.M., and Kappe, S.H.I. (2014). Interferon-Mediated
814 Innate Immune Responses against Malaria Parasite Liver Stages. Cell Reports *7*, 436–447.

815 Mueller, I., Jex, A.R., Kappe, S.H.I., Mikolajczak, S.A., Sattabongkot, J., Patrapuvich, R., Lindner, S.,
816 Flannery, E.L., Koepfli, C., Ansell, B., et al. (2019). Transcriptome and histone epigenome of
817 Plasmodium vivax salivary-gland sporozoites point to tight regulatory control and mechanisms for liver-
818 stage differentiation in relapsing malaria. International Journal for Parasitology *49*, 501–513.

819 Neefjes, J., Jongsma, M.L.M., Paul, P., and Bakke, O. (2011). Towards a systems understanding of
820 MHC class I and MHC class II antigen presentation. Nature Reviews Immunology 2011 11:12 *11*, 823–
821 836.

822 Paquet, T., le Manach, C., Cabrera, D.G., Younis, Y., Henrich, P.P., Abraham, T.S., Lee, M.C.S., Basak,
823 R., Ghidelli-Disse, S., Lafuente-Monasterio, M.J., et al. (2017). Antimalarial efficacy of MMV390048,
824 an inhibitor of Plasmodium phosphatidylinositol 4-kinase. Science Translational Medicine *9*.

825 Parussini, F., Coppens, I., Shah, P.P., Diamond, S.L., and Carruthers, V.B. (2010). Cathepsin L
826 Occupies a Vacuolar Compartment and is a Protein Maturase within the Endo/Exocytic System of
827 Toxoplasma gondii. Molecular Microbiology *76*, 1340.

828 Penaranda, C., and Hung, D.T. (2019). Single-Cell RNA Sequencing to Understand Host–Pathogen
829 Interactions. ACS Infectious Diseases *5*, 336–344.

830 Poran, A., Nötzel, C., Aly, O., Mencia-Trinchant, N., Harris, C.T., Guzman, M.L., Hassane, D.C.,
831 Elemento, O., and Kafsack, B.F.C. (2017). Single-cell RNA sequencing reveals a signature of sexual
832 commitment in malaria parasites. Nature *551*, 95–99.

833 Posfai, D., Maher, S.P., Roesch, C., Vantaux, A., Sylvester, K., Péneau, J., Popovici, J., Kyle, D.E.,
834 Witkowski, B., and Derbyshire, E.R. (2020). Plasmodium vivax Liver and Blood Stages Recruit the
835 Druggable Host Membrane Channel Aquaporin-3. Cell Chemical Biology.

836 Qu, J., Li, J., Zhang, Y., He, R., Liu, X., Gong, K., Duan, L., Luo, W., Hu, Z., Wang, G., et al. (2021).
837 AKR1B10 promotes breast cancer cell proliferation and migration via the PI3K/AKT/NF-κB signaling
838 pathway. Cell & Bioscience *11*, 163.

839 Raudvere, U., Kolberg, L., Kuzmin, I., Arak, T., Adler, P., Peterson, H., and Vilo, J. (2019). g:Profiler:
840 a web server for functional enrichment analysis and conversions of gene lists (2019 update). Nucleic
841 Acids Research *47*, W191–W198.

842 Real, E., Howick, V.M., Dahalan, F.A., Witmer, K., Cudini, J., Andradi-Brown, C., Blight, J., Davidson,
843 M.S., Dogga, S.K., Reid, A.J., et al. (2021). A single-cell atlas of Plasmodium falciparum transmission
844 through the mosquito. Nature Communications 2021 12:1 *12*, 1–13.

845 Reid, A.J., Talman, A.M., Bennett, H.M., Gomes, A.R., Sanders, M.J., Illingworth, C.J.R., Billker, O.,
846 Berriman, M., and Lawniczak, M.K.N. (2018). Single-cell RNA-seq reveals hidden transcriptional
847 variation in malaria parasites. ELife *7*, 1–29.

848 Robinson, L.J., Wampfler, R., Betuela, I., Karl, S., White, M.T., Li Wai Suen, C.S.N., Hofmann, N.E.,
849 Kinboro, B., Waltmann, A., Brewster, J., et al. (2015). Strategies for understanding and reducing the

850 Plasmodium vivax and Plasmodium ovale hypnozoite reservoir in Papua New Guinean children: a
851 randomised placebo-controlled trial and mathematical model. PLoS Medicine *12*.

852 le Roch, K.G., Johnson, J.R., Florens, L., Zhou, Y., Santrosyan, A., Grainger, M., Yan, S.F., Williamson,
853 K.C., Holder, A.A., Carucci, D.J., et al. (2004). Global analysis of transcript and protein levels across
854 the Plasmodium falciparum life cycle. Genome Research *14*, 2308–2318.

855 Rosenthal, P.J. (2011). Falcipains and Other Cysteine Proteases of Malaria Parasites. Advances in
856 Experimental Medicine and Biology *712*, 30–48.

857 Roth, A., Maher, S.P., Conway, A.J., Ubalee, R., Chaumeau, V., Andolina, C., Kaba, S.A., Vantaux, A.,
858 Bakowski, M.A., Thomson-Luque, R., et al. (2018). A comprehensive model for assessment of liver
859 stage therapies targeting Plasmodium vivax and Plasmodium falciparum. Nature Communications *9*,
860 1837.

861 Ruberto, A.A., Bourke, C., Merienne, N., Obadia, T., Amino, R., and Mueller, I. (2021a). Single-cell
862 RNA sequencing reveals developmental heterogeneity among Plasmodium berghei sporozoites.
863 Scientific Reports *11*, 4127.

864 Ruberto, A.A., Bourke, C., Vantaux, A., Maher, S.P., Jex, A., Witkowski, B., Snounou, G., and Mueller,
865 I. (2021b). Single-cell RNA sequencing of Plasmodium vivax sporozoites reveals stage- and species-
866 specific transcriptomic signatures. BioRxiv 2021.11.24.469176.

867 Sà, J.M., Cannon, M. v., Caleon, R.L., Wellems, T.E., and Serre, D. (2020). Single-cell transcription
868 analysis of Plasmodium vivax blood-stage parasites identifies stage- and species-specific profiles of
869 expression. PLOS Biology *18*, e3000711.

870 Salas, F., Fichmann, J., Lee, G.K., Scott, M.D., and Rosenthal, P.J. (1995). Functional expression of
871 falcipain, a Plasmodium falciparum cysteine proteinase, supports its role as a malarial hemoglobinase.
872 Infection and Immunity *63*, 2120.

873 Sattabongkot, J., Yimamnuaychoke, N., Leelaudomlipi, S., Rasameesoraj, M., Jenwithisuk, R.,
874 Coleman, R.E., Udomsangpetch, R., Cui, L., and Brewer, T.G. (2006). Establishment of a human
875 hepatocyte line that supports in vitro development of the exo-erythrocytic stages of the malaria parasites
876 Plasmodium falciparum and P. vivax. Am. J. Trop. Med. Hyg *74*, 708–715.

877 Scarpulla, R.C. (2002). Transcriptional activators and coactivators in the nuclear control of
878 mitochondrial function in mammalian cells. Gene *286*, 81–89.

879 Schäfer, C., Dambrauskas, N., Steel, R.W., Carbonetti, S., Chuenchob, V., Flannery, E.L., Vigdorovich,
880 V., Oliver, B.G., Roobsoong, W., Maher, S.P., et al. (2018). A recombinant antibody against
881 Plasmodium vivax UIS4 for distinguishing replicating from dormant liver stages. Malaria Journal *17*,
882 370.

883 Schäfer, C., Roobsoong, W., Sattabongkot, J., Mikolajczak, S.A., and Kappe, S.H.I. (2020). A
884 Humanized Mouse Model for Plasmodium vivax to Test Interventions that Block Liver Stage to Blood
885 Stage Transition and Blood Stage Infection. IScience *23*, 101381.

886 Schäfer, C., Zanghi, G., Vaughan, A.M., and Kappe, S.H.I. (2021). Plasmodium vivax Latent Liver
887 Stage Infection and Relapse: Biological Insights and New Experimental Tools. Annual Review of
888 Microbiology *75*.

889 Shannon, P., Markiel, A., Ozier, O., Baliga, N.S., Wang, J.T., Ramage, D., Amin, N., Schwikowski, B.,
890 and Ideker, T. (2003). Cytoscape: A Software Environment for Integrated Models of Biomolecular
891 Interaction Networks. Genome Research *13*, 2498–2504.

892 Singh, A.P., Buscaglia, C.A., Wang, Q., Levay, A., Nussenzweig, D.R., Walker, J.R., Winzeler, E.A.,
893 Fujii, H., Fontoura, B.M.A., and Nussenzweig, V. (2007). Plasmodium Circumsporozoite Protein
894 Promotes the Development of the Liver Stages of the Parasite. Cell *131*, 492–504.

895 Stuart, T., Butler, A., Hoffman, P., Hafemeister, C., Papalexi, E., Mauck, W.M., Hao, Y., Stoeckius, M.,
896 Smibert, P., and Satija, R. (2019). Comprehensive Integration of Single-Cell Data. Cell *177*, 1888-
897 1902.e21.

898 Tarun, A.S., Peng, X., Dumpit, R.F., Ogata, Y., Silva-Rivera, H., Camargo, N., Daly, T.M., Bergman,
899 L.W., and Kappe, S.H.I. (2008). A combined transcriptome and proteome survey of malaria parasite
900 liver stages. Proceedings of the National Academy of Sciences *105*, 305–310.

901 Tharyan, R.G., Annibal, A., Schiffer, I., Laboy, R., Atanassov, I., Weber, A.L., Gerisch, B., and Antebi,
902 A. (2020). NFYB-1 regulates mitochondrial function and longevity via lysosomal prosaposin. Nature
903 Metabolism *2*, 387–396.

904 Toro-Moreno, M., Sylvester, K., Srivastava, T., Posfai, D., and Derbyshire, E.R. (2020). RNA-Seq
905 Analysis Illuminates the Early Stages of Plasmodium Liver Infection.

906 Traag, V.A., Waltman, L., and van Eck, N.J. (2019). From Louvain to Leiden: guaranteeing well-
907 connected communities. Scientific Reports *9*, 1–12.

908 Tsai, H.H., Lai, H.Y., Chen, Y.C., Li, C.F., Huang, H.S., Liu, H.S., Tsai, Y.S., and Wang, J.M. (2017).
909 Metformin promotes apoptosis in hepatocellular carcinoma through the CEBPD-induced autophagy
910 pathway. Oncotarget *8*, 13832.

911 Tucker, M., Valencia-Sanchez, M.A., Staples, R.R., Chen, J., Denis, C.L., and Parker, R. (2001). The
912 transcription factor associated Ccr4 and Caf1 proteins are components of the major cytoplasmic mRNA
913 deadenylase in Saccharomyces cerevisiae. Cell *104*, 377–386.

914 Ungureanu, E., Killick-Kendrick, R., Garnham, P.C.C., Branzei, P., Romanescu, C., and Shute, P.G.
915 (1976). Prepatent periods of a tropical strain of Plasmodium vivax after inoculations of tenfold dilutions
916 of sporozoites. Transactions of the Royal Society of Tropical Medicine and Hygiene *70*, 482–483.

917 Vembar, S.S., Droll, D., and Scherf, A. (2016). Translational regulation in blood stages of the malaria
918 parasite Plasmodium spp.: systems-wide studies pave the way. Wiley Interdisciplinary Reviews. RNA
919 *7*, 772.

920 Vijayan, K., Wei, L., Glennon, E.K.K., Mattocks, C., Bourgeois, N., Staker, B., and Kaushansky, A.
921 (2021). Host-targeted Interventions as an Exciting Opportunity to Combat Malaria. Chemical Reviews
922 *121*, 10452–10468.

923 Voorberg-van der Wel, A., Roma, G., Gupta, D.K., Schuierer, S., Nigsch, F., Carbone, W., Zeeman,
924 A.M., Lee, B.H., Hofman, S.O., Faber, B.W., et al. (2017). A comparative transcriptomic analysis of
925 replicating and dormant liver stages of the relapsing malaria parasite plasmodium cynomolgi. ELife *6*.

926 Voorberg-van der Wel, A.M., Zeeman, A.M., Nieuwenhuis, I.G., van der Werff, N.M., Klooster, E.J.,
927 Klop, O., Vermaat, L.C., Kumar Gupta, D., Dembele, L., Diagana, T.T., et al. (2020). A dual fluorescent
928 Plasmodium cynomolgi reporter line reveals in vitro malaria hypnozoite reactivation. Communications
929 Biology *3*.

930 Voronina, E., Seydoux, G., Sassone-Corsi, P., and Nagamori, I. (2011). RNA Granules in Germ Cells.
931 Cold Spring Harbor Perspectives in Biology *3*.

932 Wang, C., Yan, R., Luo, D., Watabe, K., Liao, D.-F., and Cao, D. (2009). Aldo-keto Reductase Family
933 1 Member B10 Promotes Cell Survival by Regulating Lipid Synthesis and Eliminating Carbonyls. The
934 Journal of Biological Chemistry *284*, 26742–26748.

935 Wang, S.M., Lin, H.Y., Chen, Y.L., Hsu, T.I., Chuang, J.Y., Kao, T.J., and Ko, C.Y. (2019).
936 CCAAT/enhancer-binding protein delta regulates the stemness of glioma stem-like cells through
937 activating PDGFA expression upon inflammatory stimulation. Journal of Neuroinflammation *16*, 1–12.

938 White, N.J. (2011). Determinants of relapse periodicity in Plasmodium vivax malaria. Malaria Journal
939 *10*, 297.

940 White, M., Amino, R., and Mueller, I. (2017). Theoretical Implications of a Pre-Erythrocytic
941 Plasmodium vivax Vaccine for Preventing Relapses. Trends in Parasitology *33*, 260.

942 White, M.T., Walker, P., Karl, S., Hetzel, M.W., Freeman, T., Waltmann, A., Laman, M., Robinson,
943 L.J., Ghani, A., and Mueller, I. (2018). Mathematical modelling of the impact of expanding levels of
944 malaria control interventions on Plasmodium vivax. Nature Communications 2018 9:1 *9*, 1–10.

945 World Health Organization (2021). World malaria report 2021.

946 Yokomizo, T., Izumi, T., Takahashi, T., Kasamal, T., Kobayashis, Y., Satos, F., Taketanill, Y., and
947 Shimizu, T. (1993). Enzymatic Inactivation the Porcine Kidney O f Leukotriene B4 by a Novel Enzyme
948 Found in PURIFICATION AND PROPERTIES OF LEUKOTRIENE Bq 12-
949 HYDROXYDEHYDROGENASE*. THE JOURNAL OF BIOLOGICAL CHEMISTRY *268*, 18128–
950 18135.

951 Youn, J.Y., Dyakov, B.J.A., Zhang, J., Knight, J.D.R., Vernon, R.M., Forman-Kay, J.D., and Gingras,
952 A.C. (2019). Properties of Stress Granule and P-Body Proteomes. Molecular Cell *76*, 286–294.

953 Zheng, G.X.Y., Terry, J.M., Belgrader, P., Ryvkin, P., Bent, Z.W., Wilson, R., Ziraldo, S.B., Wheeler,
954 T.D., McDermott, G.P., Zhu, J., et al. (2017). Massively parallel digital transcriptional profiling of single
955 cells. Nature Communications *8*, 14049.

956

Figure 1

A

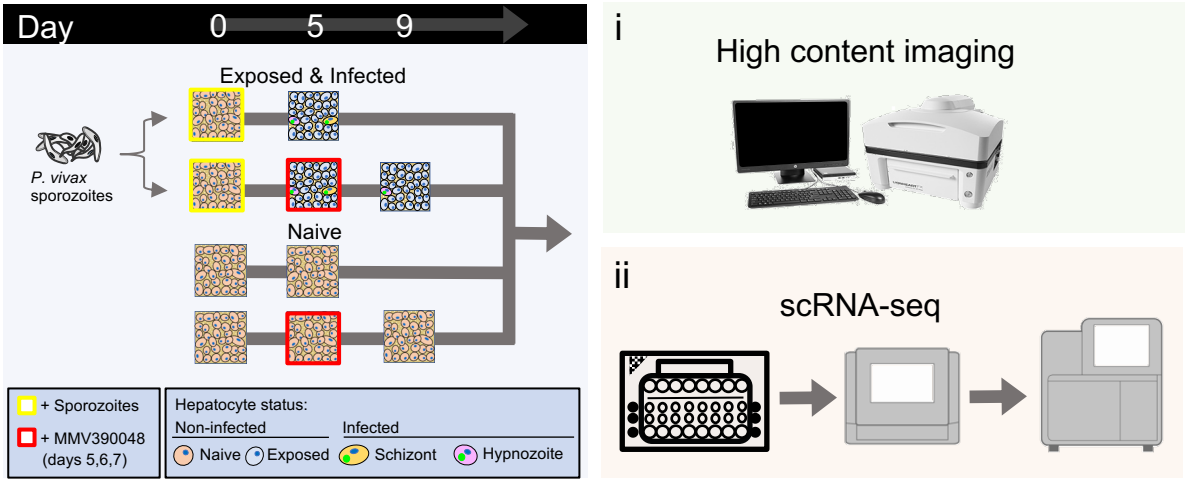


B

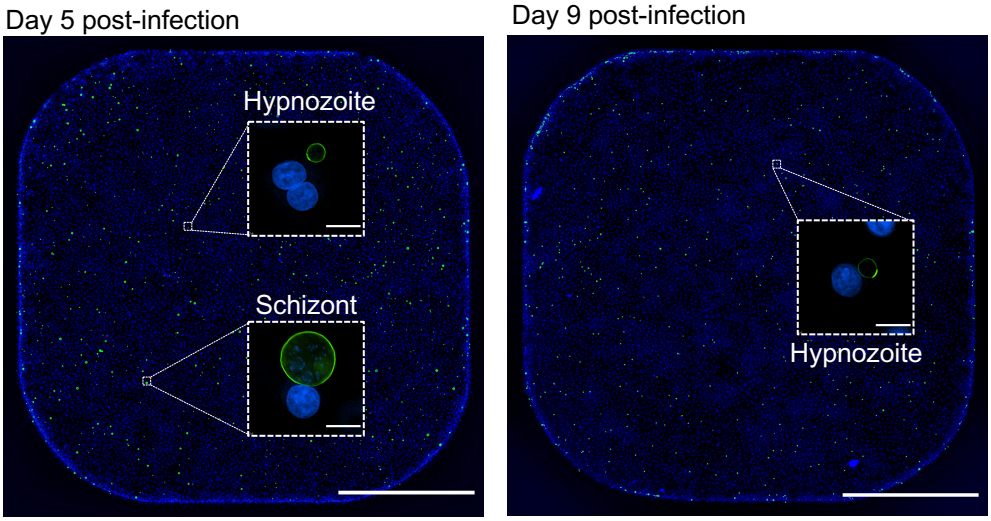


C

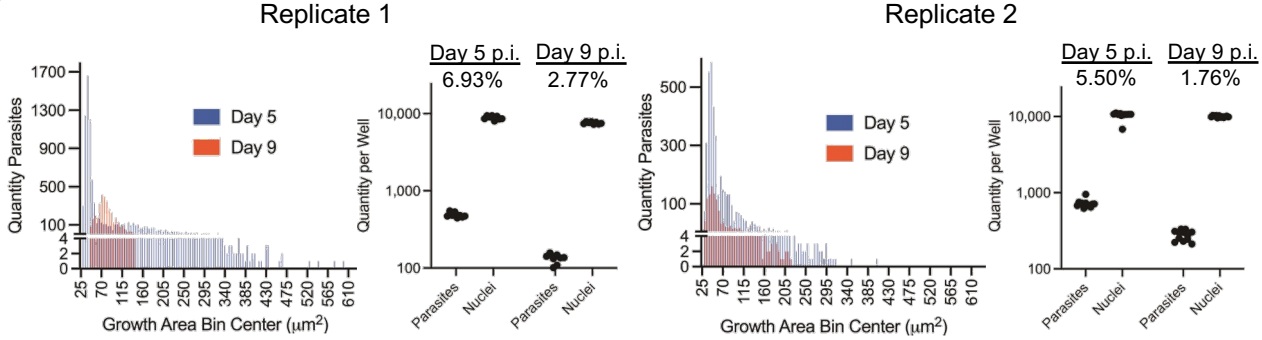


**Figure 1. Design and validation of detection of *P. vivax* liver stages using high-content imaging and scRNA-seq.** (A) Schematic illustrating the sample preparation and data generation pipeline used to assess *P. vivax* liver stage infection rates and gene expression. (B) Representative high content images of primary hepatocytes infected with *P. vivax* on day 5 (left) and day 9 (right) post-infection (p.i). Images were captured from one well from a 384-well plate with a 4x objective. Inset: one field of view (white dashed box) from the same well captured with a 20x objective. Cells were stained with DAPI (blue) and *Pv*UIS4 (green). White bar represents 1mm, inset bars represent 10μm. Images are representative of replicate 1. (C) Histogram displaying the distribution of parasite growth areas fixed at day 5 or day 9 post-infection (left) and net quantity of parasites and hepatocyte nuclei (right). Net infection rate is indicated for each endpoint. Growth and infection metrics are shown for both replicates.

Figure 2

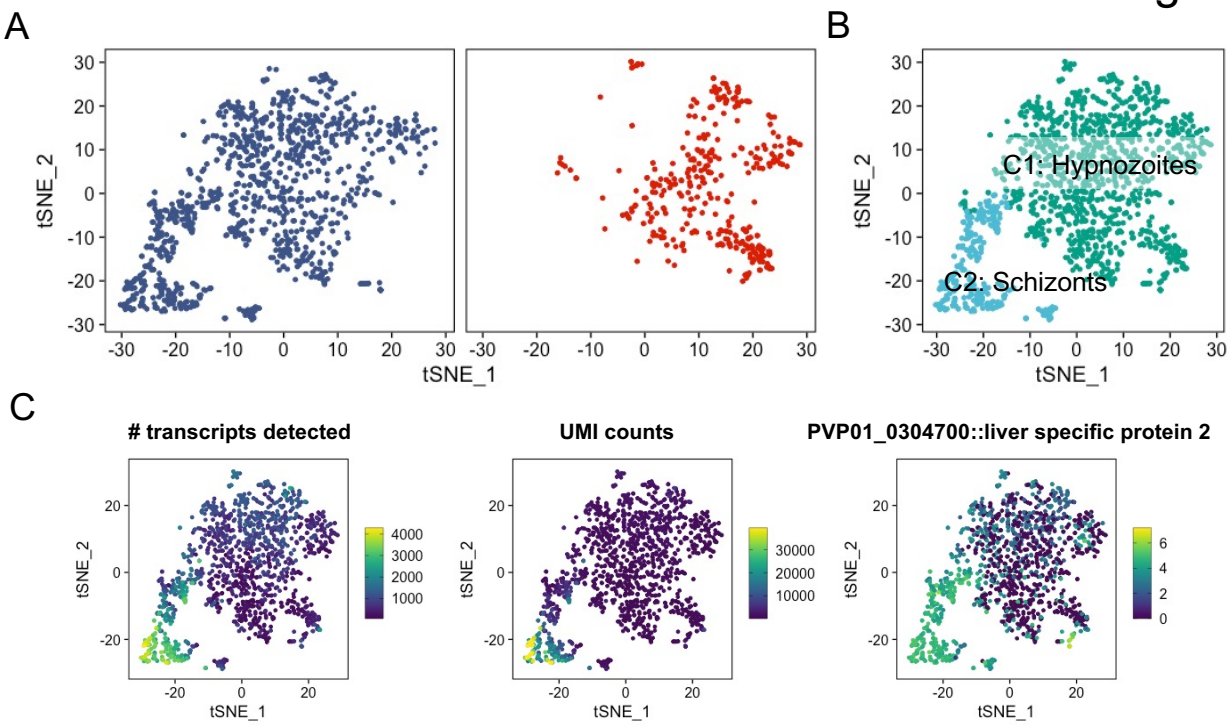


**Figure 2. Low dimensional representation of *P. vivax* schizont and hypnozoite transcriptomes** (A) t-SNE plots of integrated *P. vivax* liver stage scRNA-seq data facteted by parasites isolated on day 5 (right) and day 9 (left) post-infection. (B) t-SNE plot of *P. vivax* liver stage data colored by parasites encoding for putative hypnozoites (C1) and schizonts (C2). (C) t-SNE plots of *P. vivax* liver stage scRNA-seq data colored by number of transcripts detected (left), UMI counts (middle), and the expression of the schizont marker, LISP2 (PVP01_0304700) (right). Scales: absolute count (left, middle), normalized expression (right).

Figure 3

A

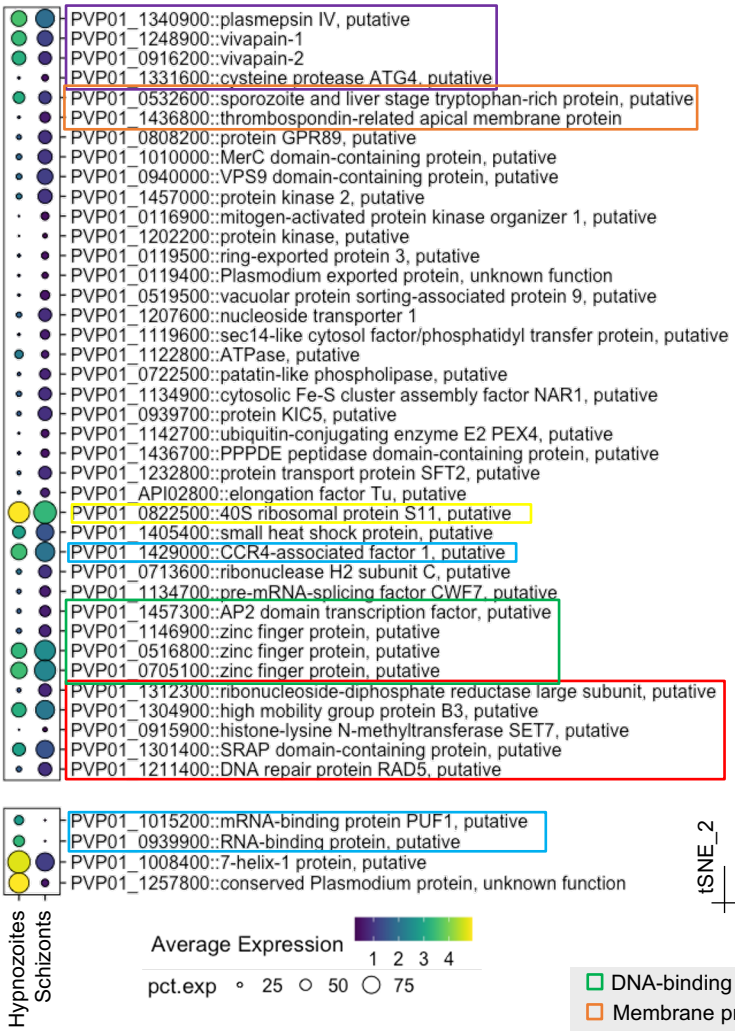


B

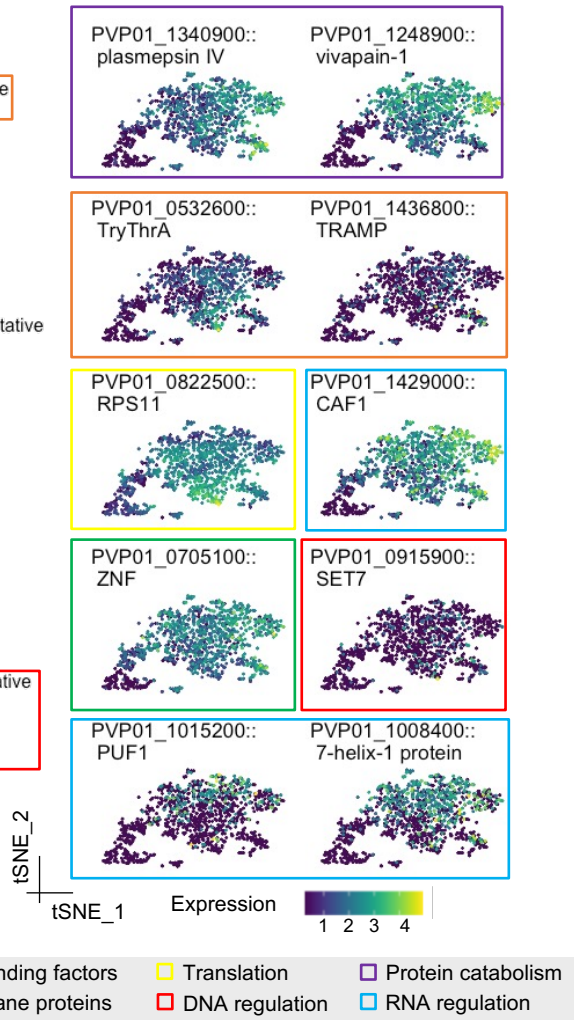


C

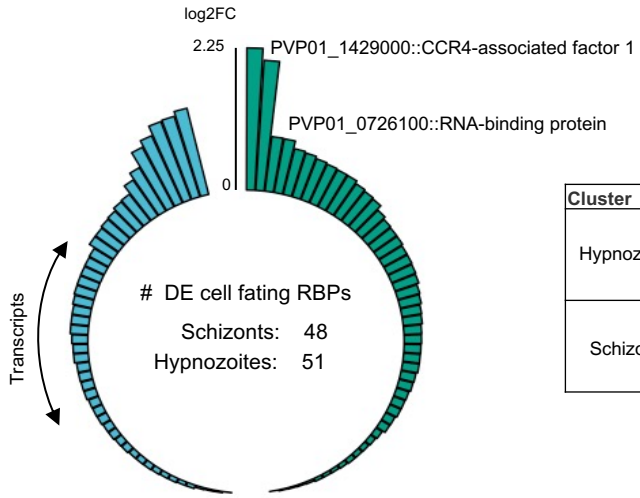


| Cluster | GO Term | Adj P |
|---|---|---|
| Hypnozoites | CCR4-NOT complex | 2.20e-9 |
| | Nucleus | 1.22e-2 |
| | P body | 2.28e-2 |
| | Regulation of gene expression | 1.97e-6 |
| Schizonts | Eukaryotic translation initiation factor 3 complex | 5.22e-6 |
| | RNP complex | 2.35e-5 |
| | Translation preinitiation complex | 1.46e-4 |
| | Translation | 7.83e-7 |

**Figure 3. *P. vivax* hypnozoites have distinct transcriptomic signatures**. (A) Dot plots showing transcripts that distinguish all hypnozoites from schizonts. The size of the dot corresponds to the percentage of cells that transcript was detected per condition, colored by average expression. Differentially expressed transcripts were identified using Seurat's FindMarker function (Wilcoxon rank-sum test, adjusted p values < 0.01). (B) tSNE plots of liver stages colored by transcripts displaying greater levels in hypnozoites. Colored boxes in A and B indicate the family or canonical biological process that the transcript is associated with. Scale: normalized expression; pct. exp: percent of cells expressing transcript. (C) Number of transcripts in schizonts and hypnozoites identified as cellula fating RBPs (left) and GO term enrichment of this subset. Adj P: Bonferroni adjusted p value.

Figure 4

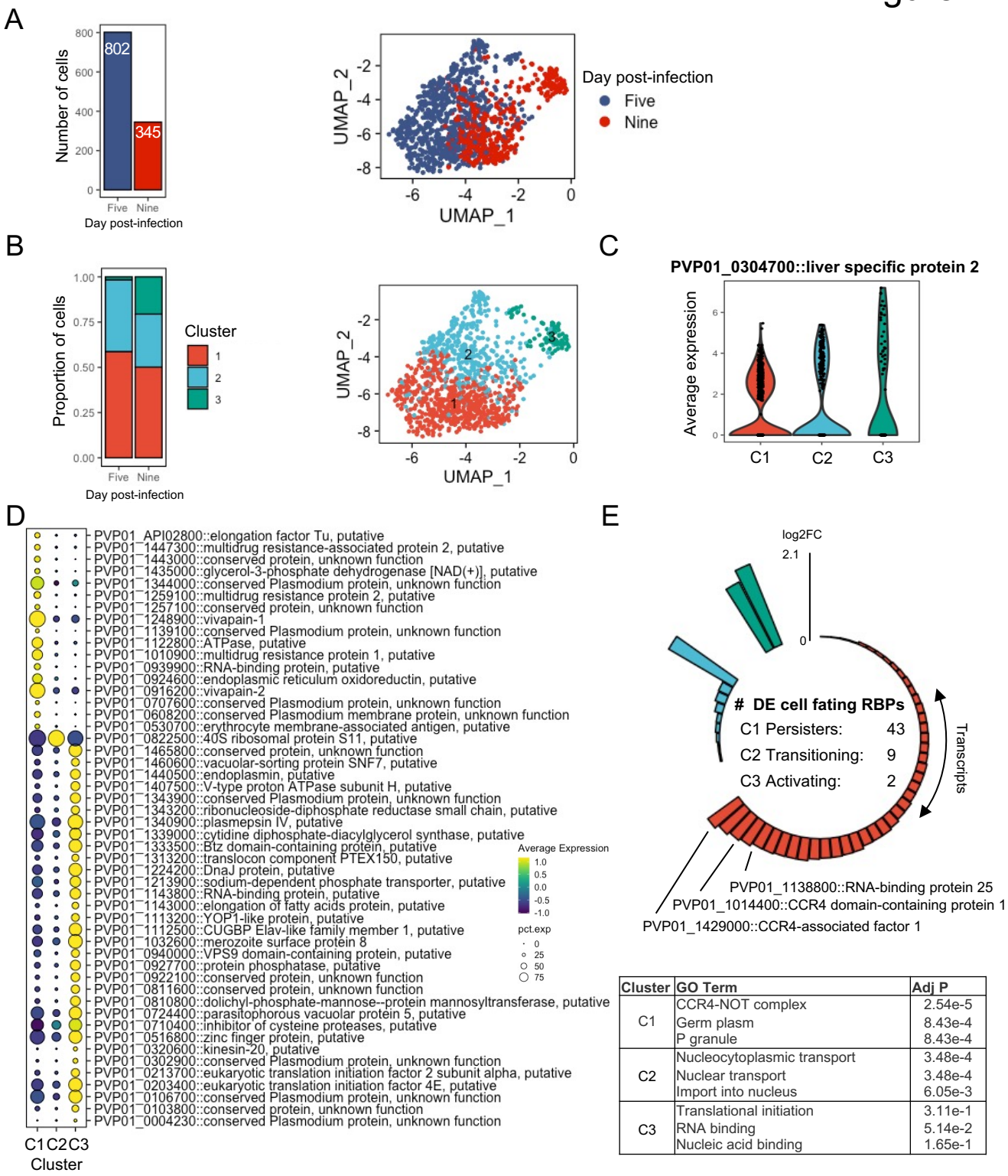


| Cluster | GO Term | Adj P |
|---|---|---|
| C1 | CCR4-NOT complex | 2.54e-5 |
| | Germ plasm | 8.43e-4 |
| | P granule | 8.43e-4 |
| C2 | Nucleocytoplasmic transport | 3.48e-4 |
| | Nuclear transport | 3.48e-4 |
| | Import into nucleus | 6.05e-3 |
| C3 | Translational initiation | 3.11e-1 |
| | RNA binding | 5.14e-2 |
| | Nucleic acid binding | 1.65e-1 |

**Figure 4. Transcriptomic signatures of reactivating and persister hypnozoites.** (A) Number of hypnozoites assessed (left) and UMAP of cells identified as hypnozoites colored by day of collection. (B) Proportion of cells in clusters on days 5 and 9 post-infection (left) and UMAP of hypnozoites colored by cluster. (C) Violin plot showing the expression of LISP2 in each cluster. (D) Dot plot showing markers that distinguish hypnozoites in each cluster. The size of the dot corresponds the percentage of cells in the expressing the gene of interest, colored by scaled normalized expression of the transcript in each cluster. Marker transcripts were identified using Seurat's AllFindMarkers function. Wilcoxon rank-sum test, average $\log_2 FC > 1$, adjusted p value < 0.01. (E) Number transcripts in each cluster encoding for cellular fating RBPs sorted by their average log2FC relative to the other clusters (top) and GO Term enrichment of transcripts in each cluster (bottom). Adj P: Bonferroni adjusted p value.

Figure 5

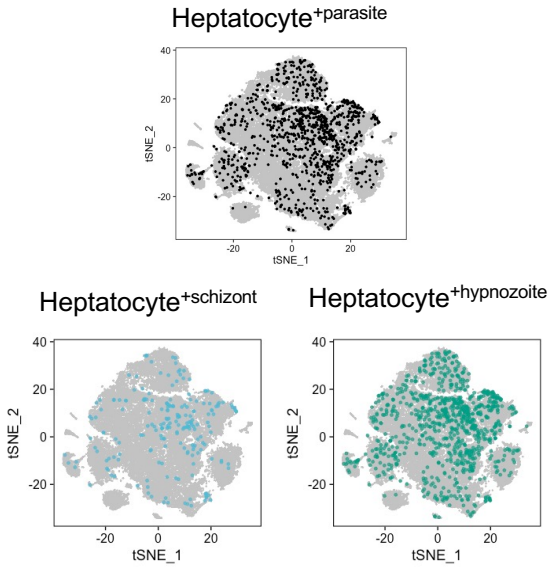


**Figure 5. Analysis of host-pathogen transcriptional signatures in *P.vivax*- infected and non-infected hepatocytes.** t-SNE plots of hepatocytes faceted by infection status. Grey, noninfected (naive and exposed) hepatocytes; light blue, hepatocytes infected with schizonts; teal, hepatocytes infected with hypnozoites.

Figure 6

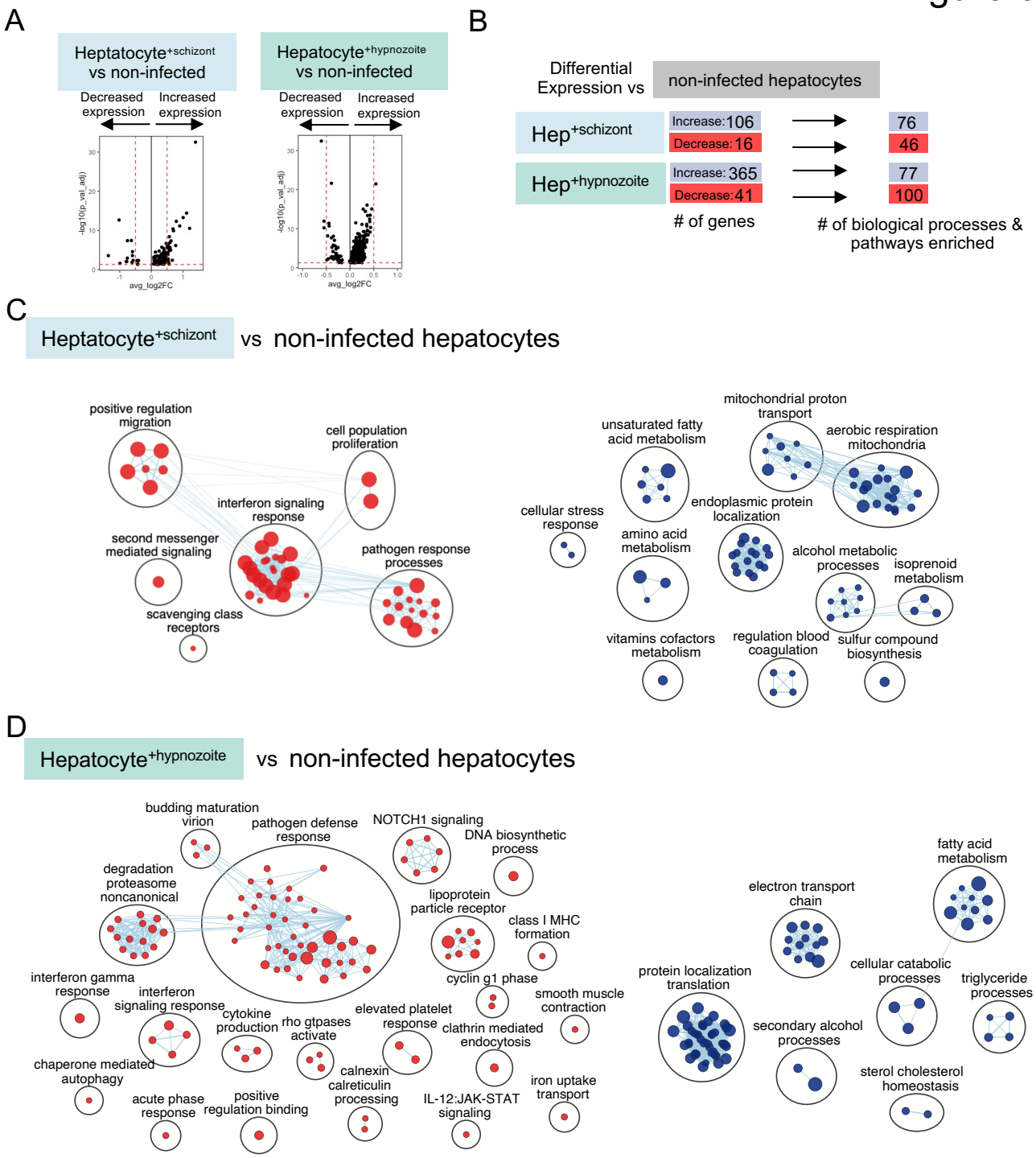


**Figure 6. Analysis of host transcriptional signatures in *P. vivax* infected hepatocytes.** (A) Volcano plots showing changes in gene expression in infected hepatocytes versus non infected (Wilcoxon rank sum, adjusted p value < 0.05). Positive fold change (FC) values represent genes with greater expression, and negative FC values represent genes with decreased expression. Dashed horizontal red lines: adjusted p value = 0.05; dashed vertical red lines: $\log_2 FC = 0.5$. (B) Summary of differential gene expression data shown in the volcano plots and of the enrichment analyses. Hep: hepatocyte. (C) Enrichment map of cellular processes and pathways associated with hepatocyte infection with *P. vivax* schizonts. (D) Enrichment map of cellular processes and pathways associated with hepatocyte infection with *P. vivax* hypnozoites. For the maps depicted panels C and D, node size is proportional to the number of genes identified in each gene set (minimum 3 genes/gene set); each node represents a distinct biological process or pathway derived from gene with decreased expression (red) or increased expression (blue) versus non-infected cells; and edges (blue lines) represent the number of genes overlapping between two processes or pathways.

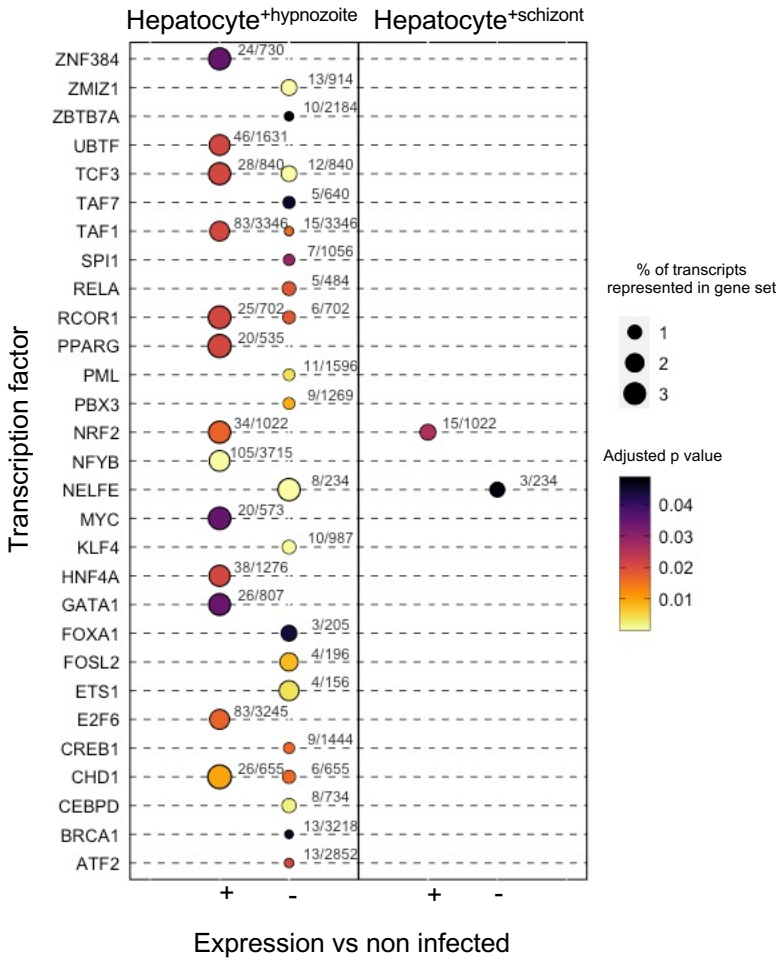


**Figure 7. Transcription factor enrichment in hepatocytes infected with schizonts or hypnozoites.** Dot plot of transcription factors enriched in Hepatocyte$^{+hypnozoite}$ (left) or Hepatocyte$^{+schizont}$ sets (right). Positive (+) enrichment derived from genes displaying greater expression versus non-infected hepatocytes; negative (-) enrichment derived from genes displaying decreased expression versus noninfected hepatocytes. ENCODE (Feingold et al., 2004) and ChEA (Lachmann et al., 2010) consensus transcription factors from ChIP-X (downloaded from Enrichr (Kuleshov et al., 2016)).